Linköping University | Department of Physics, Chemistry and Biology
Master Thesis, 60 hp | Educational Program: Chemistry
Spring 2021 | LITH-IFM-A-EX—21/3948—SE

Homebuilt Reactor Design and Atomic Layer Deposition of Metal Oxide Thin Films

Pamburayi Mpofu

Examiner, Professor Henrik Pedersen
Supervisor, Associate Professor Urban Forsberg

LINKÖPINGS UNIVERSITET

A thesis submitted in partial satisfaction of

the requirements for the degree of

MASTER OF SCIENCE

in

CHEMISTRY

Specialization: Materials Science

by

Pamburayi Mpofu

Department of Physics, Chemistry and Biology (IFM)
Faculty of Science and Engineering (Institute of Technology) (LITH)
Linköping University, Sweden

Linköping, Sweden, June 2021

Supervisor

Associate Prof. Urban Forsberg

Department of Physics, Chemistry and Biology (IFM)

Linköping University

Linköping, Sweden

Examiner

Prof. Henrik Pedersen

Department of Physics, Chemistry and Biology (IFM)

Linköping University

Linköping, Sweden

Opponent

Pentti Niiranen

Department of Physics, Chemistry and Biology (IFM)

Linköping University

Linköping, Sweden

"It looks like our long run led rather to a start than to a completion – I am deeply impressed by the huge advance that has followed in the atomic layer deposition technology and the scope of its applications." - *Dr. Tuomo Suntola, 2014*

Abstract

This research thesis covers work done on building an atomic layer deposition (ALD) reactor followed by the development and optimization of an ALD process for indium oxide thin films on crystalline silicon substrates from new precursors using this new homebuilt cost-effective tool. This work describes the design, building and testing of the ALD system using an indium triazenide precursor and water in a novel precursor combination. The reactor was built to be capable of depositing films with comparable results to commercially built systems.

Indium oxide thin films were deposited as the deposition temperature was varied from 154 to 517 ^{0}C to study the effects of deposition temperature on the obtained film thicknesses and ascertain the ALD temperature window between 269-384 ^{0}C. The presence of indium oxide films was confirmed with X-ray diffraction analysis, which was also used to study their crystallinity. The films were found to have a polycrystalline structure with a cubic phase. Measurement of film thickness was performed using X-ray reflectivity which determined a growth rate of approximately 1 Å/cycle. Elemental composition was determined by X-ray photoelectron spectroscopy which confirmed contamination-free indium rich films. Scanning electron microscope imaging was used to examine the surface morphology of the films as well as thick cross-sectional thicknesses.

Since indium oxide films are potentially useful in various electronic, optical, and catalytic applications, emphasis is also placed on the accurate characterization of the chemical and physical properties of the obtained thin films. Optical and electrical properties of the produced transparent conducting oxide films were measured for transparency (and optical band gap) and electrical characterization by resistivity measurements, from UV-Vis spectrophotometry and 4-point probe data respectively. A high optical transmission >70 %, a wide band gap 3.99-4.24 eV, and low resistivity values ~0.2 mΩcm, showed that In_2O_3 films have interesting properties for various applications confirming indium oxide a key material in transparent electronics.

Acknowledgements

The research leading to results of this thesis work was carried out and supported by The Pedersen Research Group, led by Professor Henrik Pedersen in the Department of Physics, Chemistry and Biology (IFM) at Linköping University in Sweden between September 2020 and June 2021 as part of my 2-year MSc in Chemistry journey that began in August 2019.

I would like to express my big thanks to Prof. Pedersen for introducing me to the world of CVD-ALD, welcoming and awarding me the opportunity to conduct research work with his team.

I am also totally grateful to my supervisor and tutor Ass. Professor Urban Forsberg. I appreciate his never-ending professional support, mentorship, very constructive and fruitful cooperation, and cheerful attitude since the first day of my thesis work. I do not think I could have had a better mentor. Thank you, Urban, for all your help!

During my project, I had the privilege of working with brilliant scientists in the research group. It is because of their fruitful collaboration that this work led to the result of publishable scientific work. I would want to thank these colleagues for their support, helpfulness, creativity, patience, and friendship, particularly my office mates Polla Rouf (thanks for your priceless assistance, the XRD, SEM, XPS and various instrumentation that you taught me) and Pentti Niiranen, for the fun office spirit. Working in this CVD-ALD research group has been a privilege and great fun. I wish to thank the former and current members of the group for creating such a wonderful work environment.

A big thanks goes to all the other MSc Chemistry students, class of 2021, at IFM for maintaining an extraordinarily friendly and pleasurable working atmosphere.

I gratefully acknowledge the financial support of the Swedish Institute through the Swedish Institute Scholarship for Global Professionals (SISGP) for fully funding my 2-year MSc studies.

Finally, I want to thank my family for all the support during the past 2 years that I have been in Sweden studying at Linköping University. I am grateful for all the prayers, wishes and encouragement from my parents Anos and Elizabeth. Last, but certainly not least, I wish to thank and appreciate my wife Amina for all the love and understanding, and our son Kayden for being the sunshine of my life.

Linköping, June 2021

Pamburayi Mpofu

Table of Contents

Appendices

Table of Figures

List of Tables

List of Abbreviations

3D	Three dimensional
Å	Angstrom (10^{-8}cm or 10^{-10}m)
ALD	Atomic layer deposition
ALE	Atomic layer epitaxy
CVD	Chemical vapor deposition
DAQ	Data acquisition
DI/DO	Digital Input/ Digital Output
EBE	Electron beam evaporation
EPC	Electric pneumatic converter
GPC	Growth per cycle
GUI	Graphical user interface
IFM	Department of Physics, Chemistry and Biology
LabVIEW	Laboratory virtual instrument engineering workbench
MAX	Measurement & automation explorer
MS	Magnetron sputtering
NC	Normally closed (valve)
NI	National Instruments
NPT	National Pipe Thread (American National Standard Pipe Thread standards for threaded pipes and pipe fittings)
PLD	Pulsed laser deposition
PTFE	Polytetrafluoroethylene
SEM	Scanning electron microscopy
SS	Stainless steel
TCO	Transparent conducting oxide
VI	Virtual instrument
UV-Vis	Ultraviolet-visible light (spectrophotometry)
XPS	X-ray photoelectron spectroscopy
XRD	X-ray diffraction
XRR	X-ray reflectivity

1. INTRODUCTION

1.1 Background

The need to get an atomic layer deposition (ALD) reactor available and ready to start testing of a range of newly invented metal precursors in making metal oxide thin films resulted in an additional ALD tool being desired. This therefore resulted in a concept being developed where some tool components were ordered, others fabricated, and a manual was created for ease of operation, assembling and tool layout. A control system for the ALD reactor was created in LabVIEW to regulate the thin film deposition process.

ALD is a chemical gas-phase thin film synthesis technique that can produce thin films with exceptional conformality, excellent uniformity of film thickness over large area substrates and accurate control of film thickness in the sub-nanometer range.[1] The origin of these features is a result of the unique film growth mechanism based on sequential and self-limiting surface chemical reactions that enables precise film control at atomic scale.[2]

Thin films are material layers which are limited to the nanometer scale in thickness. Thin film synthesis by ALD has attracted significant interest due to the continuing scaling down of microelectronic devices. This miniaturization of devices requires a corresponding reduction in the device features like thickness to achieve high performance. To enable all useful features of ALD in thin films deposition, the reactor design and the precursor chemistry must be studied, developed and above all, understood.

The goal of this thesis work is to develop a simple and cost-effective thermal ALD system that fulfills similar requirements to the ALD tool which is currently in use at the Department of Physics, Chemistry and Biology (IFM) by the Pedersen research group. The plasma enhanced tool in use currently is exclusively used for group 13 nitrides, hence the need to design and develop this new reactor, and then study the ALD chemistries that can be used to deposit metal oxide thin films to begin with.

Plasma enhanced ALD, which uses a plasma source to create ions and radicals, to enhance chemical reactions towards film growth is the most widely used technique as an alternative to thermal ALD these days. This is mainly because, even though it has a complicated reactor configuration, its lower processing temperatures are a catch.

However, thermal ALD, which is the conventional mode of ALD, uses energy provided thermally by heating the substrate or the entire deposition chamber.

The focus of this work lies in this thermal ALD process design and development, which consists of designing how the reactor will be built, purchasing the parts, and building the reactor, the choice of metal precursor molecules used and different process parameters that affect the chemical and physical properties of the obtained metal oxide thin films. As materials, most metal oxide films are semiconducting, and they also absorb visible light.[3] Therefore, these materials are very interesting and are potentially useful in various electronic, optical, and catalytic applications.[4]

1.2 Motivation of study

Cost effective homebuilt ALD systems have been reported before, e.g., in 2014 graduate students at Central Michigan University constructed two reactors, each for less than USD 10,000 (just under SEK 90,000). Lubitz *et al.*[5] fabricated these reactors where one was a horizontal hot walled system with a vacuum pumping system, and the other was a vertical cold walled system equipped with a quartz crystal microbalance for *in-situ* growth studies. These reactors had comparable results to commercial systems.

To deposit metal oxide films in this work, I therefore decided to design and develop a homebuilt hot-walled horizontally aligned ALD reactor as the basis of my ALD tool. This is because a hot-walled reactor is simple to build, as it requires basically only a tube and an oven. By using this design, it simplifies the development of the system reducing many complexities that can be found in other types of reactor systems. This also allowed me to design a system at low cost by reusing existing equipment as well as sourcing cheaper components. A LabVIEW program that was coded by former students doing bachelor thesis work[6] to control the valve sequencing, was customized by the author to allow synthesis of metal oxides.

In_2O_3 is an example of III-VI transparent conducting oxide (TCO) materials that have a wide band gap, hence have been the subject of significant interest particularly in the photovoltaic and optoelectronic industry because they combine unique transparent and conducting properties.[7] The investigation in this study was motivated by this unique combination of electrical and optical properties that has led numerous researchers to investigate thoroughly on the growth and properties of III oxides. For example, In_2O_3 is a highly conducting semiconductor material with a band gap between 3-4 eV, a key property of high transparency in the visible region and high reflectivity in the infrared region.[8] So, the discovery of our own novel metal triazenide precursors has made this investigation even more interesting.

Therefore, contribution of this work towards advancing the fields of nanomaterials and thin film technology consisted of an initial ALD process development study for In_2O_3 thin films. Processes with this specific combination of precursors to form In_2O_3 are reported for the first time in this thesis.

1.3 Objectives

An ALD system and process that was developed is presented using the newly discovered tris(1,3-diisopropyltriazenide)indium(III) and water for the formation of In_2O_3 thin films. In the process, I aimed to obtain pure In_2O_3 films at a wide range of deposition temperatures. The growth characteristics were to be investigated within a wide temperature range followed by the chemical, physical, optical, and electrical properties of the In_2O_3 films. Therefore, this work was carried out with the following objectives in mind:

i) Designing and building a homebuilt and customized atomic layer deposition reactor system.

ii) Using cost-effective methods and components to build the reactor that must have a computerized control system to regulate the deposition process.

iii) Experimental verification of the reactor capability to deposit metal oxide thin films using newly invented precursors. In_2O_3 films were to be synthesized and characterized in detail as a proof-of-concept study.

iv) Optimization of ALD parameters for the deposition of In_2O_3 thin films using tris(1,3-diisopropyltriazenide) indium (III) and water, to demonstrate the effectiveness of the ALD method to create metal oxide thin films.

v) Preparing and characterization of the deposited films using different analytical methods and techniques available in materials science.

1.4 Thesis overview

This thesis has a two-pronged approach. First, is the description of how the tool was designed, set up, laid out and assembled, which components were needed, their respective quantities and how the tool with its LabVIEW control code worked to control the deposition process. Second, the thesis reports the experimental tests done on newly invented potential ALD precursors to see if they can successfully make oxide films. So, it is in this second part of the thesis where experimental work done in the lab, film deposition and film characterization are described and explained. Here, emphasis is placed on characterization of the chemical and physical properties of the obtained thin films.

The contents of this thesis are organized in the following manner. This Chapter 1 has just introduced the goal of the project, the motivation, why and how the project will be executed. Chapter 2 gives the theoretical background and fundamentals of ALD, some of the previous studies done, key properties of metal oxide thin films as well as some applications. Chapter 3 explains how the ALD reactor system is designed and assembled. Chapter 4 describes the experimental verification of the designed tool by ALD of In_2O_3 thin films, process description and obtained film characterization. Chapter 5 discusses the obtained results from the different experimental characterization techniques employed throughout the work. In the same Chapter, I summarize the main results of the ALD process development studies conducted in the course of this work. Finally, concluding remarks are given as a summary and outlook in Chapter 6.

2. ATOMIC LAYER DEPOSITION

2.1 Background to thin films by ALD

Historically, the concept of ALD was first proposed under the name molecular layering in the Soviet Union by Prof. V. B. Aleskovskii in his Ph.D. thesis published in 1952[9] followed by a few publications from him and his co-workers in the 1960s.[10,11,12] However, the name molecular layering has remained relatively less known and poorly cited to this day. Hence most credit goes to Finland's Dr. Tuomo Suntola for popularly developing ALD in 1974 under the name atomic layer epitaxy (ALE), whereby the growing film was intended to display the same crystalline structure as the underlying substrate.[13] The principles of operation of this technique have evolved over the years from ALE to ALD because the interest in amorphous films in electronic devices has also strongly increased.[14]

ALD is a deposition and thin film growth technique based on sequential, self-limiting surface reactions. This method is a gas phase deposition process, which uses alternating saturated surface gas-to-solid chemical reactions.[15] It occurs by chemical reactions of two or more precursors pulsed alternately into a chamber where a substrate is placed at a given deposition temperature to enable materials (thin films) deposition on the substrate's surface, layer by layer.

Thin films are commercially important and of interest for many applications. ALD films are currently mainly used in the microelectronics industry, and this includes transparent conducting oxides, high-*k* gate oxides in consumer electronics,[16] photovoltaic buffer layers in thin film solar cells,[17,18] sensors,[19] optical devices,[20] and flat panel displays.[21,22] Metal oxide thin films have been prepared by various methods, such as magnetron sputtering[23,24,25,26], electron beam evaporation[27,28], pulsed laser deposition[29], chemical vapor deposition (CVD)[30,31] and ALD[32,33] before.

Even though physical and chemical vapor deposition techniques continue to dominate the field of electronic thin film deposition, the continuous trend in downscaling of critical device dimensions means that ALD is the convenient choice as it tends to have more advantages than the rest. Its advantages include low-process temperature (generally <400^{0}C); high degree of film homogeneity; good compositional control; high conformality due to controlled layer-by-layer growth; film thickness control at atomic level; good reproducibility and straightforward scale-up; no gas phase reactions occur, favoring the usage of precursors that are highly reactive towards each other and the capability to prepare multilayer structures in a continuous process. Considering the economy of the process, ALD reactors are usually quite small, resulting in small footprints, which is good when clean room area is expensive to operate.

Table 1. Comparison of ALD capabilities vs other deposition techniques[34,35]

Parameter	ALD	CVD	MS	EBE	PLD
process temperature	good (low)	varies	good	good	good
degree of homogeneity	good (high)	good	poor	poor	poor
compositional control	good	varies	poor	poor	poor
conformality	good (high)	varies	poor	poor	poor
thickness uniformity	good	good	good	fair	fair
reproducibility	good	fair	good	fair	fair
lack of pinholes	good	good	fair	fair	fair
industrial applicability	varies	good	good	good	poor
deposition rate	poor	good	good	good	good
step coverage	good	varies	poor	poor	poor
film density	good	good	good	good	good
interface quality	good	varies	poor	fair	varies
automated multilayers	good	fair	good	fair	fair

MS = Magnetron sputtering EBE = Electron beam evaporation
PLD = Pulsed laser deposition CVD = Chemical Vapor Deposition

There are many similarities between ALD and CVD, in fact ALD is time-resolved CVD. The main difference between ALD and CVD is that there is discrete feeding of the precursor and the co-reactant in ALD. Because of the self-limiting behavior of ALD, the thickness of grown layer is mainly dependent on the number of applied cycles, rather than flow of reaction gases or time parameters. This allows the growth of thin films with precisely defined thickness and uniformity over the large area, even on the non-planar (3D) surfaces, which is one of the biggest advantages of the ALD over CVD. The adhesion of deposited material is usually good, and the deposition induced substrate damage is low.

So, in short even though ALD is a variant of CVD, but unlike CVD or other similar deposition methods, in ALD the precursors are not pumped simultaneously, they are pulsed sequentially. The distinction lies in the self-limiting characteristics for precursor adsorption, alternate and sequential introduction of the precursors and co-reactants.[36]

On the contrary, ALD has its own drawbacks and disadvantages, for example: long purge times, particularly when water is the co-reactant; low growth per cycle (GPC) values; very slow process with slow growth rate and low precursor utilization efficiency. Another concern with the ALD method is that, even though it is true of all CVD processes, this technique releases environmentally harmful chemicals during the process' half reactions. The main disadvantage in comparison to CVD is that it is a slower process that has a higher precursor consumption. However, these difficulties can be compensated for and overcome by having the right reactor design and proper precursor selection in ALD.

2.2 The ALD cycle

One ALD cycle, as shown in Fig. 1, consists of four steps: precursor pulse, purge, co-reactant pulse, and purge. The principle of ALD method is described below using a metal oxide deposition from diethylmetal precursor ($(C_2H_5)_2M$) and H_2O.

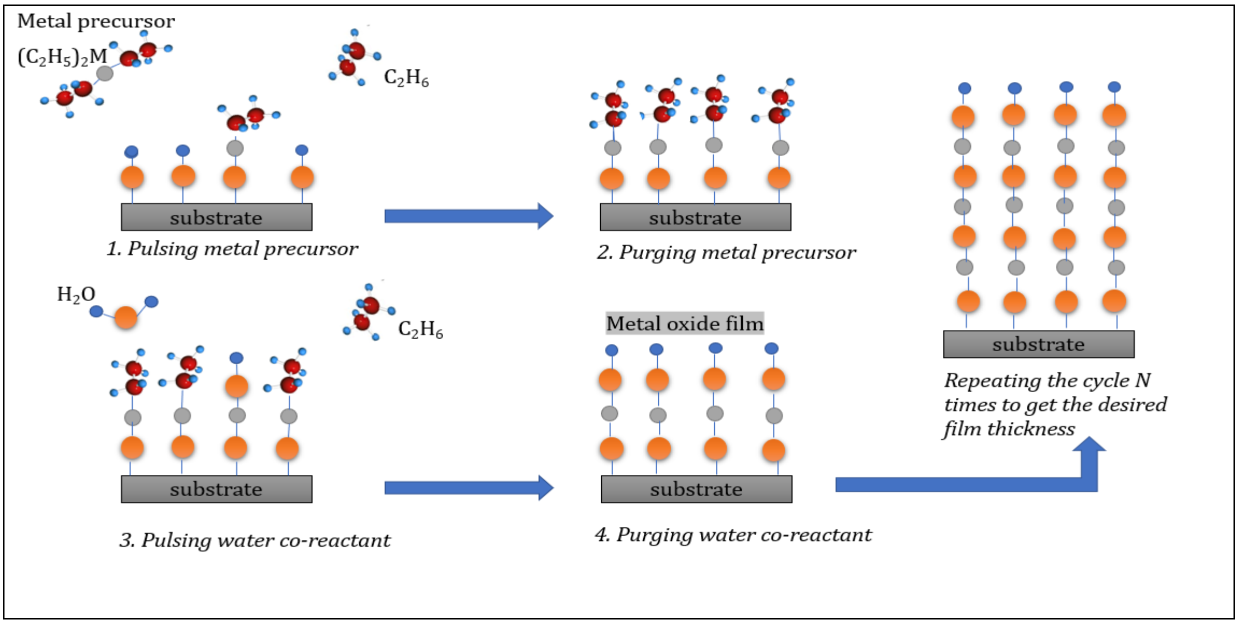

Figure 1. Illustration of a four step ALD cycle for a metal oxide thin film deposition using a metal precursor and water.

For depositing metal oxide films, one of the precursors must contain a metal atom, while the other precursor acts as the oxygen source. In ALD chemistry, where H_2O is used as the co-reactant oxygen source (like the case in this study), the primary reaction mechanism is an exchange reaction between the ligands of the metal precursor and the surface hydroxyl groups. These reactions result in a formation of new chemical bonds between metal atoms and oxygen atoms as well as the release of protonated ligands as by-products. The ligand exchange reactions can occur during both the metal precursor pulse and the H_2O pulse. A schematic of this ligand exchange mechanism is shown in Fig. 1.

2.3 Saturation curves

The most important aspect of ALD is the self-limiting adsorption of precursors and layer-by-layer deposition of the material in the case of properly chosen conditions resulting in saturative growth behavior of deposited thin films as shown in Fig. 2. Surface chemistry rules ALD processes hence precursors react through saturative surface reactions whereby films grow from the subsaturation regime until no further film growth is observed no matter how long a precursor is dosed. After saturation, precursors and reactants are well-evacuated from the reactor before pulsing the next precursor.

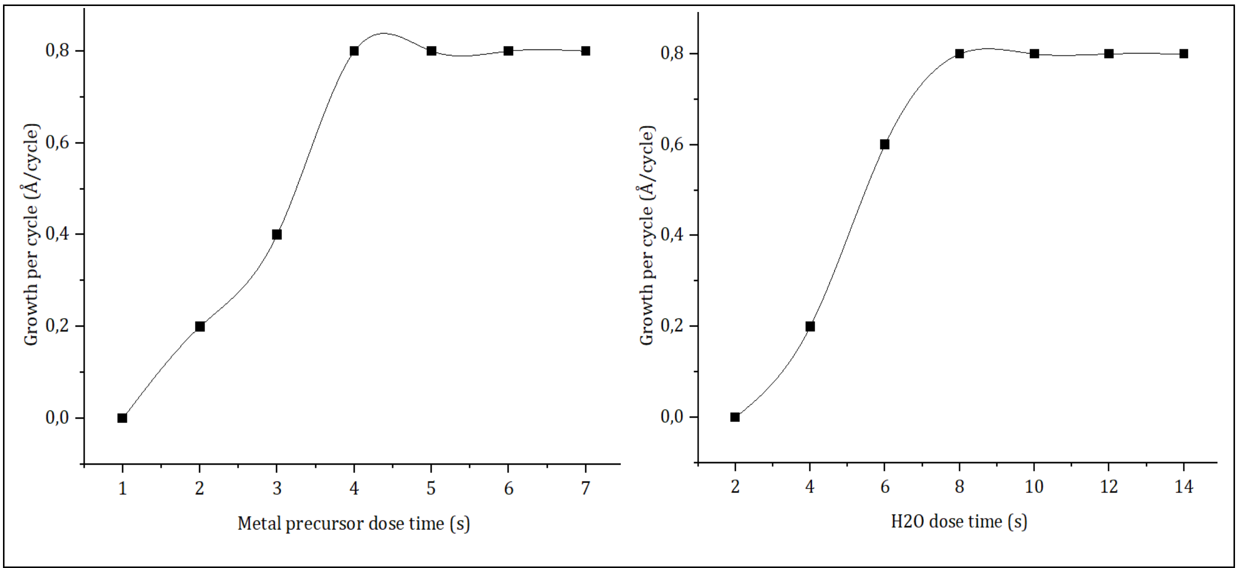

Figure 2. Schematic example of a metal oxide ALD process: saturation curves

A self-limiting chemistry as shown by these saturation curves, is an absolute must in an ALD process.

2.4 Temperature window

The temperature window is the temperature range within which the growth per cycle is insensitive to substrate temperature changes, as illustrated in Fig. 3. This temperature range where the growth is saturated depends on the specific ALD process and is also referred to as the ALD window. Because ALD exploits the binding energy difference between chemisorption and physisorption at the substrate surface[37], in this temperature window the chemisorption phenomenon is dominant. This is therefore the reason why ALD growth is a process independent of parameter changes because only an atomic layer can be adsorbed on the surface at the time.

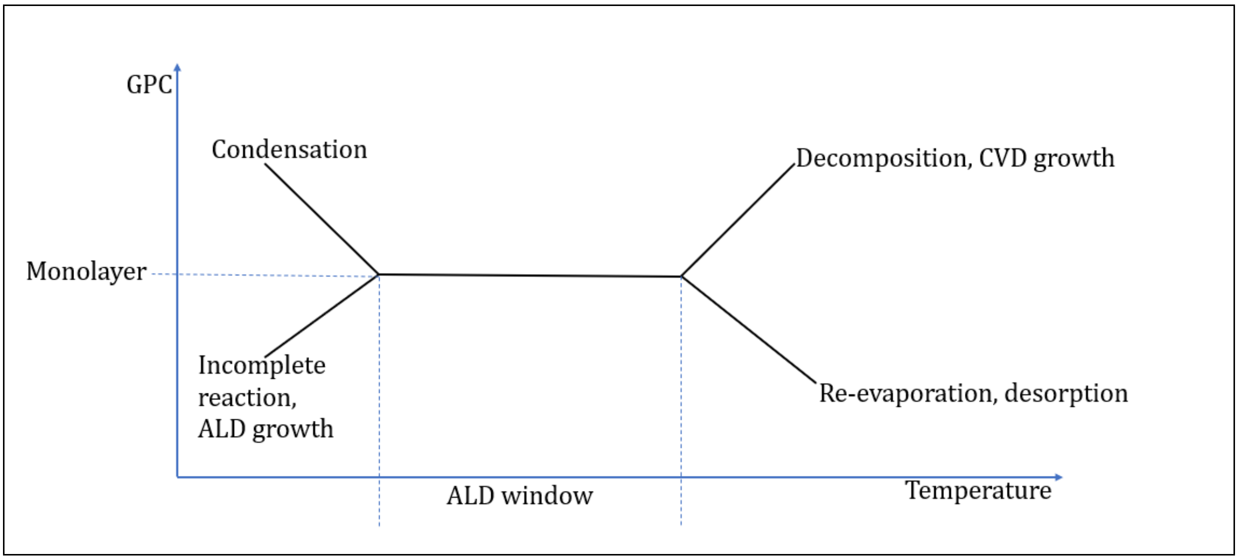

Figure 3. Dependence of the growth rate on the deposition temperature. Self-limited growth reaction occurs in the middle part of the graph, in the so called ALD window.

Since the growth process is self-limiting, the amount of precursor injected in a pulse does not affect the deposition rate (growth or thickness per cycle) if the substrate surface has been completely covered. In principle, ALD offers a deposition rate of one monolayer per ALD pulse, but this seldom happens in reality due to steric hindrance on the surface. This phenomenon gives unparalleled control over the film thickness. However, as shown in Fig. 3, the deposition rate in the early stage of an ALD process is less than a monolayer per cycle. The reasons for this are the limited number of reactive sites initially present on a substrate surface, and slow reaction kinetics due to the large size of the ligands in the case of metalorganic precursors compared to the length scale over which surface atoms are arranged on a growing thin film[38].

Thermal sensitivity of ALD is also illustrated in Fig. 3. At low temperatures there is both high and low growth rates. High growth rates indicate that there might be condensation of the reactant and low growth rate means poor reactivity of the reactant. At higher reaction temperatures exceeding the ALD window, two things can happen. There is desorption of the formed monolayer (dissociation of a surface ligands essential to activate the surface for the next reactant is happening), which results in lower growth rate. Then there is higher growth rate signifying the formation of non-volatile cracking products of reactants or surface ligands.[39] This is also known as CVD growth.

2.5 Precursor chemistry

To achieve ALD's unique characteristics and to be suitable as a practical vapor deposition process, ALD precursors must have specific properties. The main characteristics of an ideal ALD precursor are volatility, fast and reproducible vaporizing, i.e., high vapor pressure, resistance to thermal decomposition at the surface or in gas phase, high reactivity towards other precursors and volatile but not corrosive by-products (that can cause etching and tool corrosion). A good precursor must have low toxicity and be non-flammable, preventing leak related hazards. Available precursors seldom meet all the requirements but are good usually only in some respects.[40] Therefore, the selection of precursors often depends on the process objective and substrate properties. In practical applications and deposition of films there are often trade-offs between precursor properties and film quality considering the most crucial aspects described.[41]

Investigations into developing and using metal precursors with favorable surface chemistry for ALD of nitrides have been made before in the Pedersen research group and I believed the same could be done in ALD of oxides by using H_2O as the co-reactant oxygen source.

Like in many other ALD tools, this ALD system was used to enable the reaction of metal precursors with water to produce thin films of metal oxides on the surface of a silicon substrate. The precursor delivery system and control architecture were designed so that cyclic pulsating flows as defined by ALD are facilitated.

2.6 Metal oxides

Oxides of various elements have been reported more frequently in both thermal and plasma ALD literature, in comparison to nitrides, sulfides, phosphates, fluorides, and even pure elements themselves.[42] Several metal oxides have as well been reportedly deposited by ALD previously using different types of precursors: from metal halides to organometallic precursors and oxygen sources that include H_2O, hydrogen peroxide (H_2O_2), ozone (O_3) and molecular oxygen (O_2). The most frequently used oxygen sources in thermal ALD of metal oxide thin films are H_2O and O_3 and in fewer cases, O_2, "wet oxygen" (a mixture of H_2O vapor and O_2),[43] as well as primary alcohols and H_2O_2 have also been utilized.[44]

The main advantage of using H_2O as the oxygen source in metal oxide ALD is the ability to remove the metal precursor ligands intact. This approach can be used to avoid the incorporation of ligand fragments as impurities. Other advantages of H_2O include its ready availability, ease of use and non-toxicity. The disadvantages associated with H_2O-based ALD chemistry are related to extremely low and high deposition temperatures. At low temperatures (≤ 100 °C), water molecules can remain on the film surface as well as on the ALD reactor walls due to high activation energy of desorption.[45] This signifies that long purging times are required to ensure that film growth proceeds in the ALD mode. Consequently, ALD metal oxide films deposited using H_2O at low temperatures often contain an increased amount of hydrogen impurities.[46] The disadvantages of high temperature deposition are related to surface dihydroxylation, which has been noted to cause a decrease in growth per cycle (GPC) due to diminished amount of surface groups available for ligand exchange reactions.[47]

Similar metal precursors used in the deposition of nitrides were also used in the ALD of metal (III) oxides from amidinate precursors as described by Harvard University's Roy G. Gordon in his talk on '*Precursors with Metal-Nitrogen Bonds for ALD of Metals, Nitrides and Oxides*'.[48] The emphasis in my study is on a smaller sized precursor but of almost the same make-up because the smaller the size, the better the ALD. This motivated me to try depositing metal oxide films using the newly synthesized triazenide complexes which have a smaller size, with H_2O as the oxygen source.

2.7 Indium oxide

In_2O_3 is a III–VI binary oxide semiconducting material existing primarily in a cubic crystal structure. It functions as a transparent conducting oxide[49] that possesses a wide direct band gap, as mentioned earlier on, between 3–4 eV at room temperature, with high optical transparency and excellent chemical stability.[50] Among the various transparent conducting oxides, In_2O_3 has attracted tremendous attention due to its enormous applications in many fields. In_2O_3 thin films are used in several applications, including as a transparent, wide-band gap semiconductor for (opto)electronic applications[51], heat mirrors[52], electrochromic devices[53], gas sensors, catalysts, and antireflection coatings.[54] Indium oxide thin films have a unique property of optical transparency and electrical conductivity[55]; of which the electrical conductivity of these films is mainly controlled by the oxygen stoichiometry in the film.[56]

Of the ALD processes for In_2O_3 that have been developed, most if not all of them have limitations somehow. For example, early investigations in 1998, of In_2O_3 ALD using $InCl_3$ with either H_2O or H_2O_2 as the oxygen source were reported by Ritala *et al.*[57] The ALD chemistries suffered from the need for high growth temperatures (350–500 °C), the generation of corrosive HCl as the reaction byproduct, and the very low vapor pressure of the $InCl_3$ precursor, which required a sublimation temperature of 285 °C. Another issue with the $InCl_3/H_2O$ ALD chemistry, is that $InCl_3$ can etch the growing In_2O_3 layer and even changing to use of a trimethylindium (TMIn) precursor was not good either since it does not show any self-limited growth.[58]

To date, atomic layer deposition has been employed to produce In_2O_3 films based on self-limiting chemical reactions on substrate surfaces, and many indium compounds have been employed as precursors in combination with different oxidants and within different temperature windows as shown in Table 2.

Table 2. Known indium precursors and oxidants employed for ALD of In_2O_3 films.[59,60]

Indium precursor	Oxidant	ALD window (^0C)
$InCl_3$	H_2O or H_2O_2	300 – 500
TMIn	H_2O	200 – 250
TMIn	O_3	100 – 200
InCp	O_3	200 – 450
InCp	H_2O/O_2	100 – 350
InCp	H_2O_2	160 – 200
In(acac)$_3$	H_2O or O_3	165 - 220 (H_2O), 160 - 225 (O_3)
In(tmhd)$_3$	O_2 plasma	100 – 400
In[(^{i}PrN)$_2$CNR2]$_3$, R=Me, Et	H_2O	230 – 300
Et$_2$InN(TMS)$_2$	H_2O	175 – 250
INCA, DADI, TEIn	O_3	100 – 200
INCA	H_2O_2	125 – 225
DADI	H_2O	275
In(dmamp)$_3$	O_3	100 – 300
Me$_2$In(EDPA)	O_2 plasma	70 – 250
tris(N,N'-diisopropylacetamidinato) indium(III)	H_2O	150 – 275

TMIn = trimethyl indium,

InCp = cyclopentadienyl indium (I),

acac = acetylacetonate,

tmhd = 2,2,6,6-tetramethyl-3,5-heptanedionate,

In[(iPrN)$_2$CNR$_2$]$_3$ = indium-tris-guanidinates,

Et$_2$InN(TMS)$_2$ = diethyl[bis-(trimethylsilyl)amido]indium,

INCA = diethyl[1,1,1-trimethyl-N-(trimethylsilyl)silanaminato]indium,

DADI = [3-(dimethylamino)propyl]dimethyl indium,

TEIn = triethyl indium,

dmamp = 1-dimethylamino-2-methyl-2-propoxy,

Me$_2$In(EDPA) = dimethyl(N-ethoxy-2,2-dimethylpropanamido)indium.

The major breakthrough in In_2O_3 deposition by ALD using 'better' precursors was in 2018 by Kim *et al.*[61] The interesting discovery in their process was that they managed to achieve a deposition within a wide and low temperature ALD window. Thus, it is always of paramount importance to keep identifying and developing new precursors for processes. This gives a better understanding of precursor chemistry and hence better process development.

To motivate this observation, the previous study by Kim *et al* on the ALD of In_2O_3 was followed up by Rouf *et al*.[62] on the ALD of indium nitride (InN) in 2019 and both support the fact that the change of the endocyclic substituents on the respective amidinate and guanidinate backbones of the homoleptic complexes revealed a superior performance of the formamidinate derivative complexes in the corresponding processes.

But, an even more superior precursor performance is discovered when there is an electronegative nitrogen atom in the endocyclic position as proven by O'Brien *et al*. in 2020 on the invention of indium(III)triazenide for ALD of InN.[63] It is in that recent paper that the synthesis of a homoleptic In precursor, tris(1,3-diisopropyltriazenide)indium (III) was reported, and herein the author wanted to prove that an In_2O_3 ALD process can be successfully performed using the same precursor and water as the indium source and co-reactant, respectively.

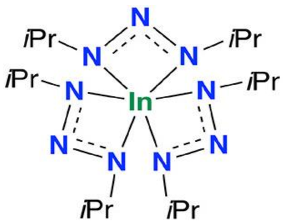

Figure 4. The Indium precursor: tris(1,3-diisopropyltriazenide) indium (III), otherwise known as indium (III) triazenide.

The distinct advantages of the triazenide precursor in Fig. 4 are higher volatility, thermal stability and better processing characteristics compared to the other common indium precursors. To the best of the my knowledge, processes with this specific combination of precursors are reported for the first time in this work.

3. ALD REACTOR AND SYSTEM DESIGN

The ALD tool that I aimed to design was a homebuilt, hot-walled, and a cross flow-type of reactor. It is horizontally aligned with a vacuum purging system. Two major sections of the system are discussed: hardware (the deposition chamber, precursor and co-reactant delivery system are discussed in detail along with the precursor bubbler designs and the rest of the design components) and software (LabVIEW) to control reactants delivery by opening and closing the four ALD valves.

No major mention is given to 'small' components like ferrules, connectors, unions, gaskets, union tees, O-rings, crosses, flanges, needle valves, couplings, and other fittings. But they will all be found in our shopping list, the bill of materials (BOM) Appendix A - 'BOM checklist of components.'

The idea is to design a reactor that can controllably, reproducibly, and safely produce thin films by controlling the following three important kinetic parameters:

i) *Process temperature* by having a heating system that heats up precursor delivery lines, chamber walls and the substrate.

ii) *Precursor partial pressure* (precursor concentration) through precursor vapor pressure and pump speed.

iii) *Reaction time* through automated periods of opening and closing of valves using LabVIEW.

3.1 Hardware

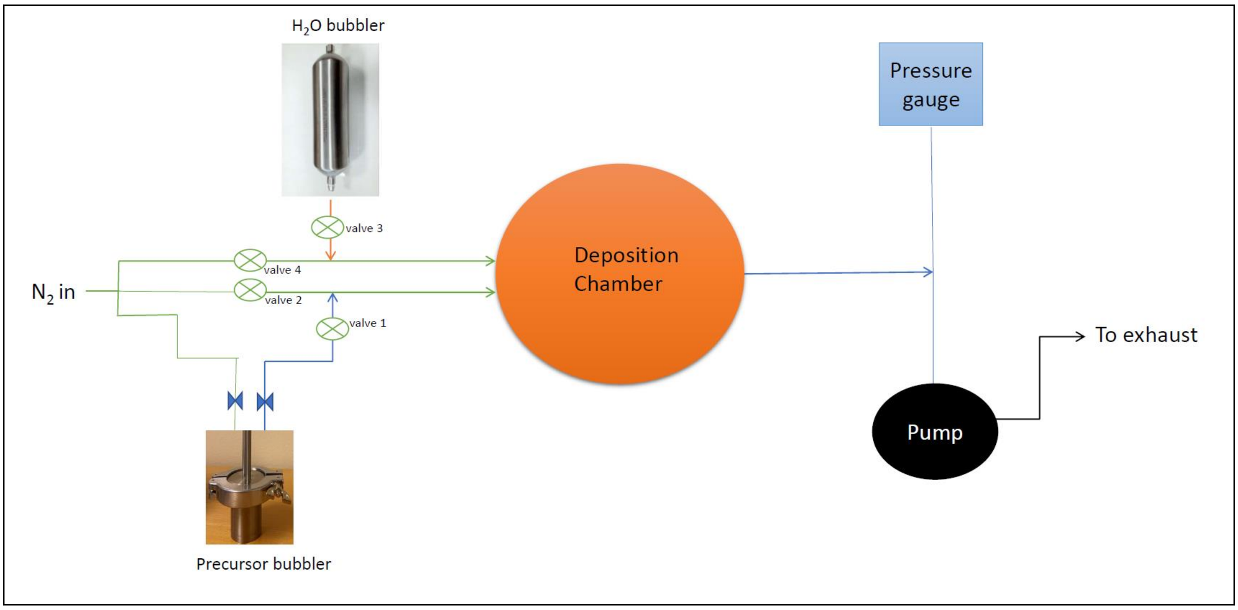

Figure 5. A schematic illustration of how the system is laid out.

All pipes and containers were designed to be able to handle a pressure or operating conditions of a high vacuum. Components in direct contact with precursors and reactants are made of acid-resistant steel or similar materials that do not react when in contact.

3.1.1 Deposition chamber

Figure 6. The deposition chamber with the new name of the tool inscribed on it – ''The Mastermind.''

The deposition chamber is a hot wall, horizontal flow chamber with a stainless tube inside that has a diagnostic access that can be opened and closed to put in or take out the sample. The chamber has an operating temperature of 1500 °C max which is a temperature the stainless tube must withstand. The material of the oven tube meets this requirement. This requirement also applies for the supporting gas lines as well as the cover for the furnace pipe and plates. The chamber walls are heated by cartridge heaters and electrical heating coils. The sample holder is heated concurrently since it is located within the vacuum chamber. The system deposition temperature is controlled by setting the required temperature on the chamber heating power controller. The reactor walls and delivery lines are always heated above precursor bubbler temperature to avoid precursor condensation.

As the stainless-steel tube in the chamber can be heated up to an operating temperature of above 200 ˚C and more, there will be great stress for the seals and rings on the couplings at the chamber outlet. It should be noted that, even if it is not 200 ˚C on the outlet, it will still be very hot enough to melt the rings hence cooling is a requirement. Therefore, water cooling is used to minimize the risk of O-rings melting.

3.1.2 Valves and precursor delivery lines

N_2 is used to carry precursor vapor from the bubbler to the deposition chamber and to purge precursor or oxidizer out of the deposition chamber. Precursor delivery lines are carefully designed to facilitate ALD mode of operation, to minimize cost, improve compactness, and facilitate portability. The system has two delivery pipes with a common line as they enter the reaction chamber.

Each line has a Flowlink pneumatic valve working as an ALD valve arranged as shown in the hardware set up in Fig. 5. Manual needle valves on the metal precursor bubbler are used to protect air-sensitive precursors from getting in contact with air during precursor transfer. Oxidant delivery is controlled by a manual switching valve connected to the bubbler, followed by an ALD valve for delivery into the reaction chamber.

Valve 1 (for metal precursor pulse) is opened momentarily, followed by valve 2 (metal precursor purging), valve 3 (H_2O oxidant pulse), and finally valve 4 (H_2O oxidant purge) in a cyclic manner. This valve configuration allows for ALD deposition mode within a single delivery system configuration.

A custom-designed LabVIEW computer control program with input/output (I/O) voltage interface electromechanically controls the series of valves which, in turn, controls N_2 pressure to the pneumatic valves in the delivery lines.

Thus, via a computer command, the open/close sequencing of delivery valves is controlled for processes happening in the ALD chamber. All valves are bolted firmly on a metal plate for rigidity and mounted right on top of the desk next to the deposition chamber for compactness. The deposition chamber, valve plates, and control system parts are so arranged to improve rigidity as shown in Fig. 7.

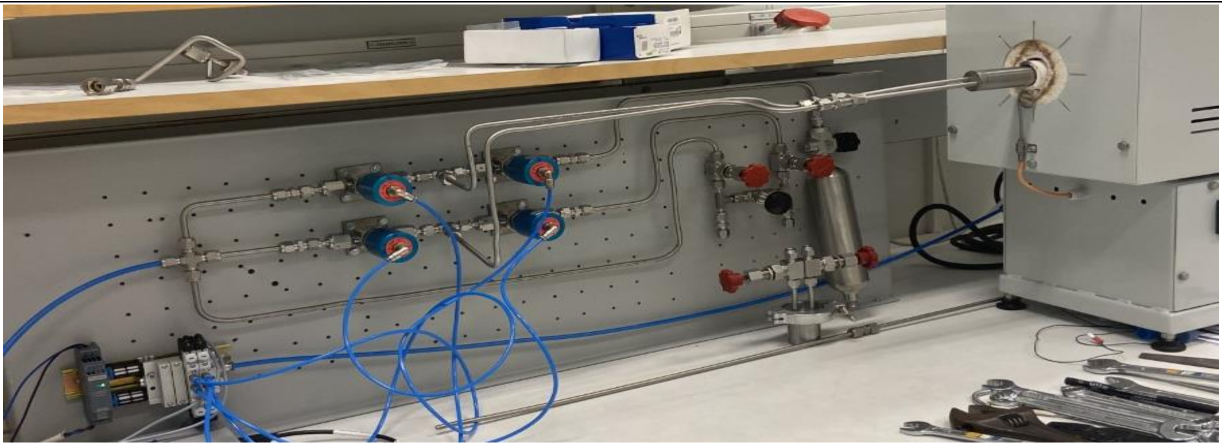

Figure 7. Valves and ultimately related components are bolted firmly on a metal plate for rigidity.

3.1.3 Bubblers

A bubbler is an evaporation chamber from where precursors are supplied with energy to get into the vapor phase. Precursors are kept in stainless steel (SS) bubblers and transported to deposition chamber through stainless-steel tubes. The metal precursor bubbler temperature is measured or controlled using a dimer so that it is just enough and does not exceed or cause decomposition of the metal precursor.

3.1.3.1 Metal precursor bubbler

Most vapor deposition systems use heated-open boat to deliver solid or low-vapor pressure liquid precursors and passivated stainless-steel bubblers for moderate to high vapor pressure liquids. In this study, a continuous flow CVD-type bubbler was used to accommodate an ALD operating mode. The precursor bubbler is fabricated from stainless steel, assembled using laser welding techniques and can be heated up to about 200 °C. A complete O-ring is used to seal the bubbler reservoir to the top cap which has two

Swagelok fittings welded onto the cap for gas in and out ports. The fittings on the cap have manual needle valves at each end. The bubbler has a dip tube for the in port. Wetted areas of the bubbler are electropolished internally and externally to minimize potential surface reactions and outgassing with the precursor.

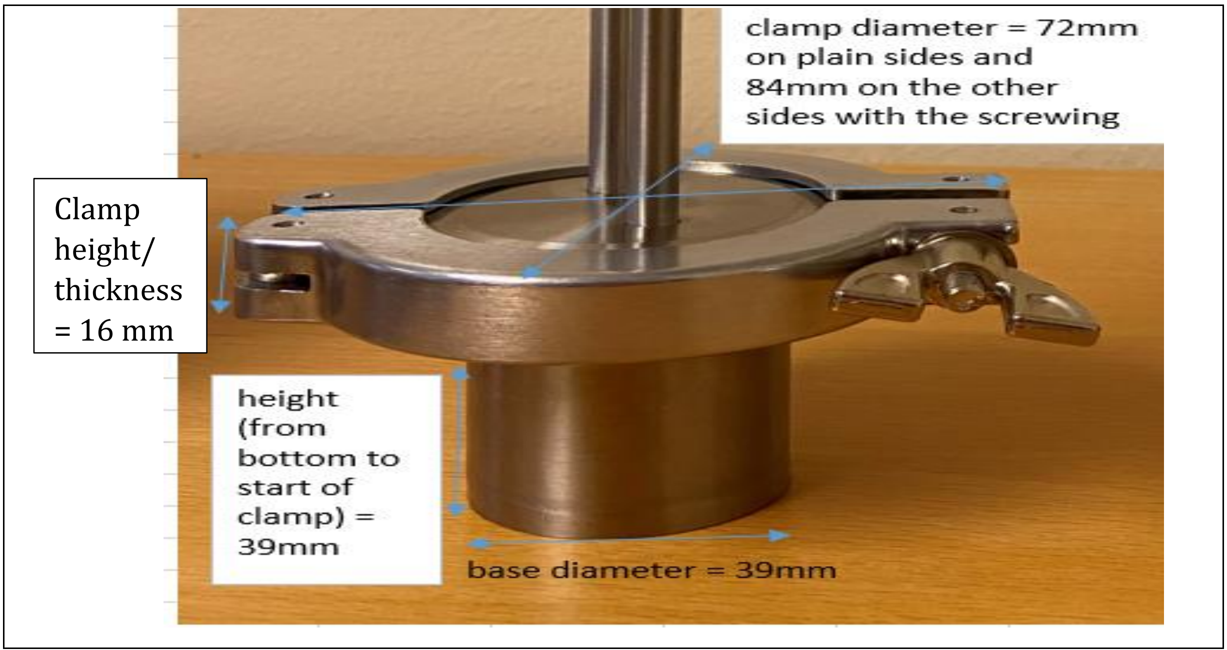

Figure 8. Stainless steel metal precursor bubbler

The bubbler can be disassembled and taken for filling in the glove box where the metal precursor is processed. This makes the requirement on the gas lines that they should be able to be closed completely to maintain vacuum in the container. One of the gas lines that enter the bubbler should run approximately 3-5 mm from the bottom. One of the gas pipelines will have a constant flow of N_2 and the other a combination of precursor and nitrogen gas which will suck up (due to the negative pressure) the heated and vaporized precursor into the deposition chamber.

3.1.3.2 Water co-reactant bubbler

This bubbler delivers water vapor to the deposition chamber. Water vapor is delivered over the head space of the water bubbler maintained at a room temperature. The water bubbler is connected to an ALD valve to deliberately avoid N_2 injection inside the water bath to reduce moisture content in the N_2 without requiring additional dilution or heating-up of downstream delivery lines to prevent water vapor condensation. In this system, no nitrogen is bubbled through the water reservoir. This arrangement reduces oxidizer purging time. The oxidizer delivery line is connected to a normally closed (NC), Flowlink ALD valve which in turn is connected to the nitrogen delivery line.

Figure 9. Water bubbler or reservoir

The bubbler in Fig. 9, a cylinder of volume 300 cm^3 with a 1/4-inch national pipe thread (NPT) female connection, a non-rotating valve, and a bottom plug was improvised to work as our water bubbler. Internal surface of the cylinder is coated with polytetrafluoroethylene (PTFE) to provide a nonstick surface, which aids in cleaning or electropolished to provide a clean internal surface with a high degree of passivation.

3.1.4 Heating tapes

Heating tapes from Hemi Heating maintained a temperature range of about 120-160 °C and able to cover the bubbler and as well as delivery lines including all pipes and valves. The four ALD valves were heated with the tape and therefore must withstand temperatures in this range and must be opened or closed without leakage.

3.1.5 Pressure gauge

An EPIGRESS pressure monitor with a digital display was used as a pressure gauge. The pressure gauge was already available in stock. It has KF16 coupling and therefore needed a coupling reduction from KF25 to KF16. To facilitate continuous stream of reactants at a set pressure, it was connected to the outlet of the deposition chamber. The pressure gauge was connected to deposition chamber outlet and covered the pressure ranges in the size 0–1000 mbar.

3.1.6 Vacuum pumping system

A VARIAN DS 302 (model 949-9325) vacuum pump connected to the deposition chamber outlet was used to give an improved deposition process with better process control. This was also available in stock. The vacuum pump controls the chamber pressure by pumping it down to the base pressure. It can create a negative pressure of 1 mbar. A stainless-steel flexi hose is connected to the pump outlet to transfer all the by-products and residual gases to the exhaust line. A mesh was fitted to prevent samples from getting into the pump. A manual valve was installed between the vacuum pump and the deposition chamber to isolate the deposition chamber during sample transfer and to regulate chamber pressure during deposition. A flexible plastic hose was used between pump and chamber to prevent pump vibration from reaching deposition chamber.

3.1.7 Sample holder

A fabricated flat stainless-steel pan was used to get the sample in and out of the deposition chamber. This sample holder was heated to control temperature of sample (deposition temperature). The sample holder must have the same requirements as the stainless-steel tube and preferably be able to handle more than one sample at a time. It is small enough to be able to pass through the KF coupling and has a hook or loop to push it in and pull it out. Of course, it must withstand temperatures above 200 ^{0}C.

3.2 Software - LabVIEW and Data Acquisition Control System

This section describes the control system in a simplified way: how a LabVIEW program was used to generate signals that control the ALD mode of operation. LabVIEW is a program based on block programming that create a graphical user interface (GUI). When LabVIEW runs a code, it sends the program signals from the computer via USB to a data acquisition unit, which in turn sends the control signal to open or close the valves. To get the computer to control the electric pneumatic converter (EPC), and hence the valves, both software and hardware are required. The data acquisition (DAQ) and EPC components used were purchased from National Instruments (NI) and FESTO, respectively.

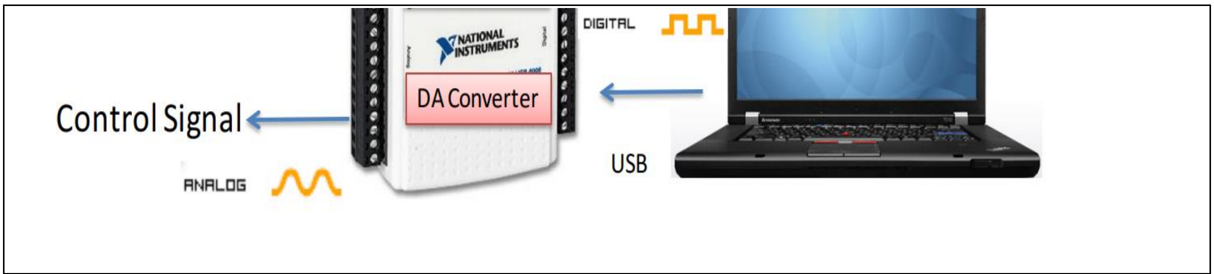

Figure 10. A DAQ unit coverts computer based digital outputs into analog control signal outputs and measured analog signal inputs into digital inputs.

3.2.1 Data acquisition system (DAQ)

DAQmx driver software is installed, configured, and used to setup the 'myDAQ' device in the measurement & automation explorer (MAX). In MAX, the myDAQ appearance is verified for the correct device name and the test panel is used to ensure that all signals are read successfully.

A combination of a Compact DAQ chassis and an 8-channel module with screw terminals from NI was used as the DAQ unit. The purpose of this unit is to generate signals for precursor control and injection diluted in the carrier gas, N_2, and the subsequent timely controlled injection into the reactor. The temporally separated injection of precursors with intermittent purges is important to suppress any gas phase reactions (standard ALD set up), which can become dominant in a dense gas phase. The system is fully computer controlled and utilizes a programmable logic controller to provide precise synchronization between precursor injection and optical data acquisition. The control system opens and closes the four valves that regulate the flow in four gas pipes. The gas pipes merge as they enter the deposition chamber as shown on the hardware section in Fig. 3. Only one valve is open at a time. At start, the time for how long the valves should be open must be determined and logged into LabVIEW for each run sequence and, if need be, is repeated for a certain number of cycles. After each precursor has gone through the tube a cleaning process takes place where only nitrogen flows through the system (purging). The DAQ unit is programmed by a LabVIEW code which sends an electrical output to the correct valve at corresponding intervals. See Fig. 11 below for an overview of how the data acquisition system is structured.

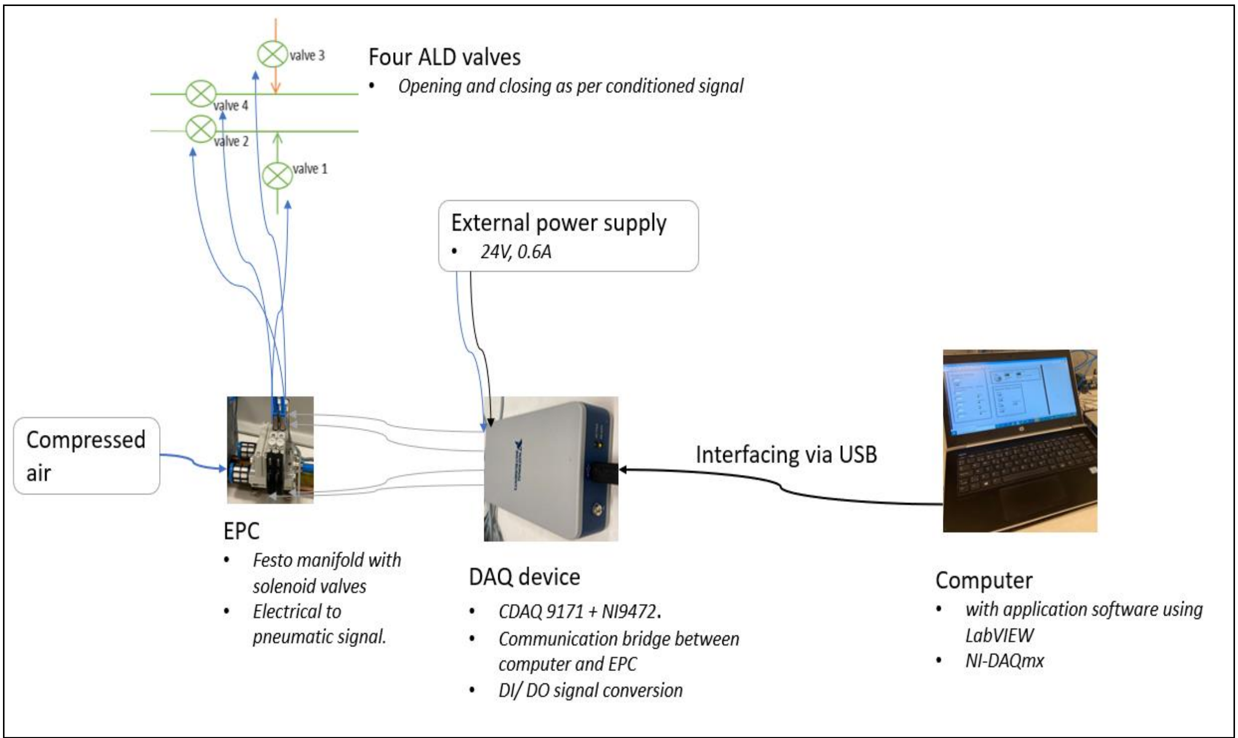

Figure 11. Hardware to software connection illustrating the overall system operational representation.

3.2.2 Electric Pneumatic Converter (EPC)

To control the system, ALD valves can be opened and closed using control gas (compressed air) via DAQ-generated digital output (DO) signals sent to the FESTO solenoid valves manifold which acts as our EPC. It converts an electrical input signal to pneumatics that pressurize the ALD valves.

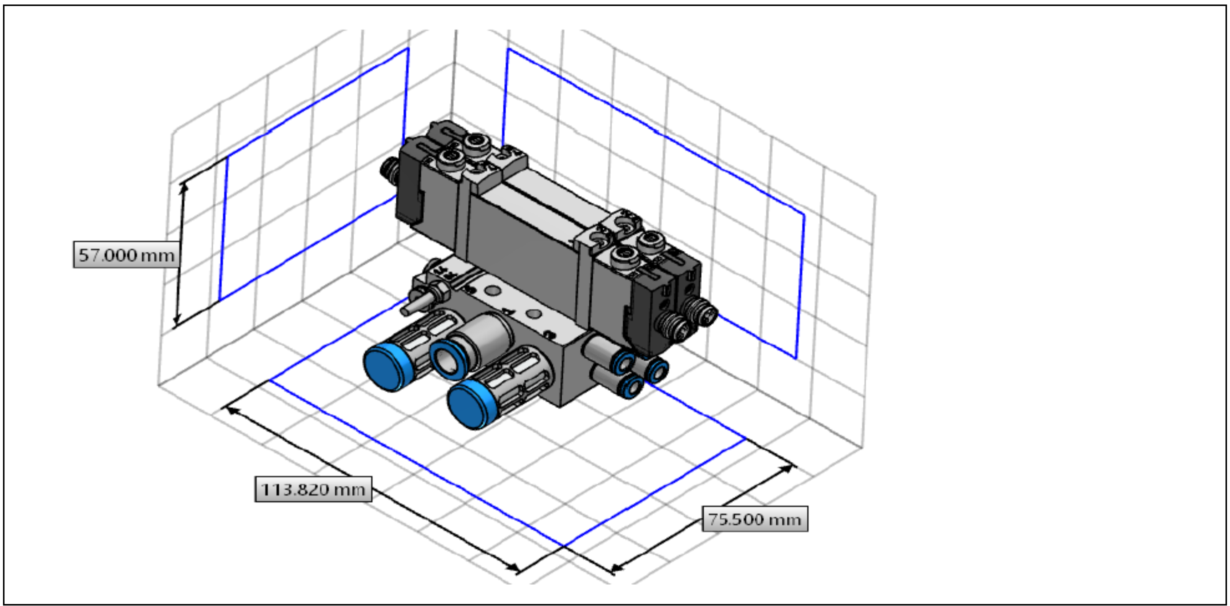

Figure 12. Electric Pneumatic Converter Unit

The outlet ports of the EPC are connected to the ALD valves in the following order:

Port 1 to Valve 1 – Metal precursor (reactant pulse)

Port 2 to Valve 2 – Cleaning Pipe 1 (purging)

Port 3 to Valve 3 – H_2O oxidant (co-reactant pulse)

Port 4 to Valve 4 – Cleaning Pipe 2 (purging)

3.2.3 LabVIEW Virtual Instrument (VI)

Laboratory Virtual Instrument Engineering Workbench (LabVIEW), an interactive platform for a visual programming language from National Instruments is defined as ‘‘a systems engineering software for applications that require test, measurement, and control with rapid access to hardware and data insights.’’[64]

LabVIEW programs are called virtual instruments (VIs). Inputs are called controls and outputs are called indicators. Each VI contains three main parts:

a) Front panel – how the user interacts with the VI,

b) Block diagram – the code that controls the program and

c) Icon/connector – the means of connecting a VI to another VI.

Controls and indicators are front panel items that you can use to interact with your program to provide input and display results.

A VI is the key element of the program and happens ‘behind the scenes.’ It considers the number of ALD cycles, precursor pulse time, precursor purge time, oxidant pulse, and oxidant purge times as inputs, and controls the four pneumatic ALD valves (V1-V4) that deliver the carrier gas, precursor, and oxidant.

When the DAQ unit is plugged into the computer, right clicking on the block diagram, and going to Express>> Input >>DAQ Assist, places the DAQ assistant to start the system. When the DAQ assistant is placed on the block diagram, a wizard automatically pops up where one configures what they want to do, i.e., if you want to read or write data, analog, or digital signals, which channel you want to use, etc. This information is later shown to the user on the LabVIEW front panel resembled by the user interface.

The actual step by step programming procedure will not be fully covered in this work, but it will be given as a basic introduction because there are many programs, functions, and subroutines that have been taken from popular programming languages like C or Basic and this takes a whole separate module to fully understand. The LabVIEW User Manual on ni.com is a good starting point for someone interested in the hands-on procedures and provides additional and important information for programming in LabVIEW.

3.2.3.1 Block diagram

LabVIEW, Version 19.0f2(64-bit), block diagram of the program used in this work is shown in Fig. 13. In a way, the block diagram resembles a flowchart.

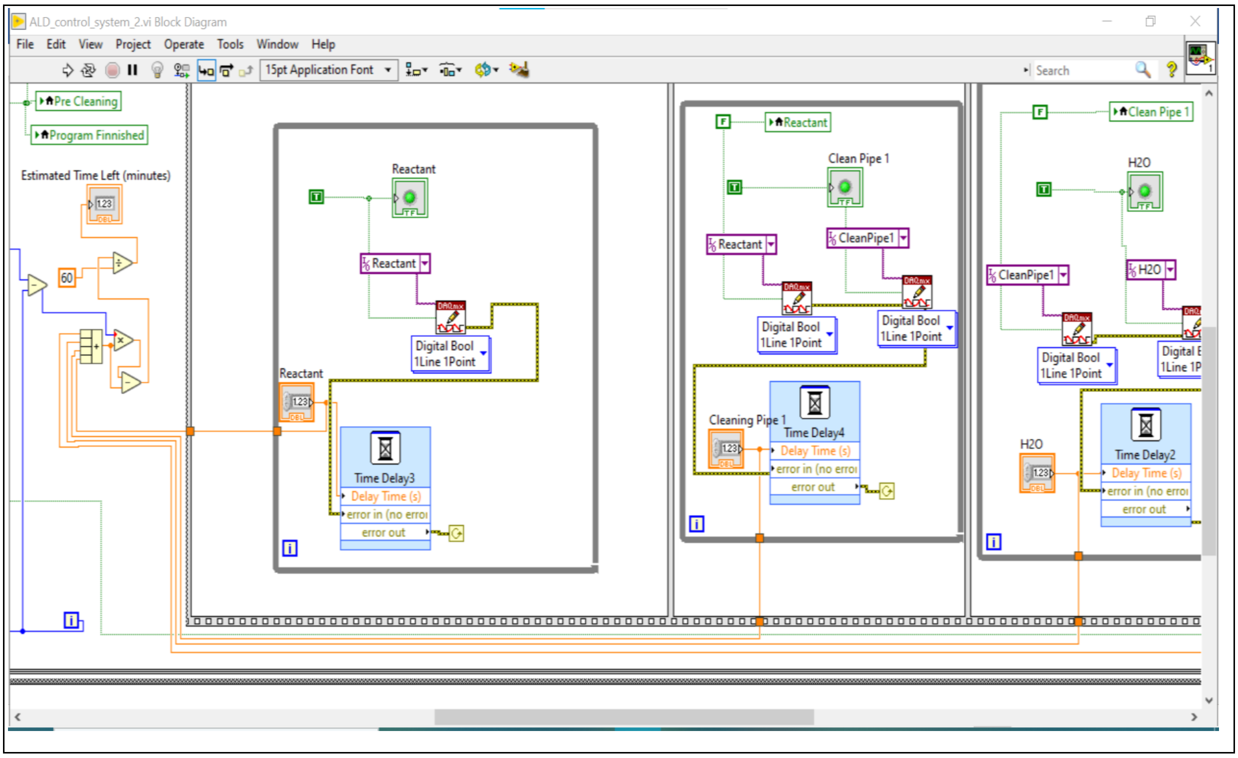

Figure 13. LabVIEW block diagram which contains the graphical code of a VI for ALD precursor delivery and pipe/line cleaning system.

When creating a VI, a terminal is created on the block diagram where an object on the front panel is created. Terminals give access to the front panel objects from the block diagram graphical code. Each terminal contains useful information about the front panel, the object it corresponds to such as, the color and symbols providing information about the data type. For example, boolean terminals are green with true or false (T/F) lettering.

Generally, blue terminals are wired to blue terminals, green to green, and so on. This is not a strict rule, e.g., a blue terminal (dynamic data) can be connected to an orange terminal (fractional value). But in most cases, one must look for a match in colors. Controls have a thick border and an arrow on the right side. Indicators have a thin border and an arrow on the left side. Logic rules apply to wiring in LabVIEW: each wire must have one source (control), and each wire may have multiple destinations (indicators).

Valve positions, T/F (True/False) for all four ALD sub-cycles or steps are stored in an “ALD recipe” in this block diagram. This valve position information is sent to boolean indicators and DAQ unit that communicates with valve hardware; whereas sub-cycle time is sent to “wait” block, that halts the LabVIEW program in the same valve positions for the specified sub-cycle time before switching to the next sub-cycle valve positions. The entire process repeats four X N times in loop to cover all four ALD sub-cycles for N number of times. The ALD program described here is however, as indicated earlier, a simplified version of the program that has few extra recipes to include “delay time before deposition” and second precursor line.

3.2.3.2 Front panel

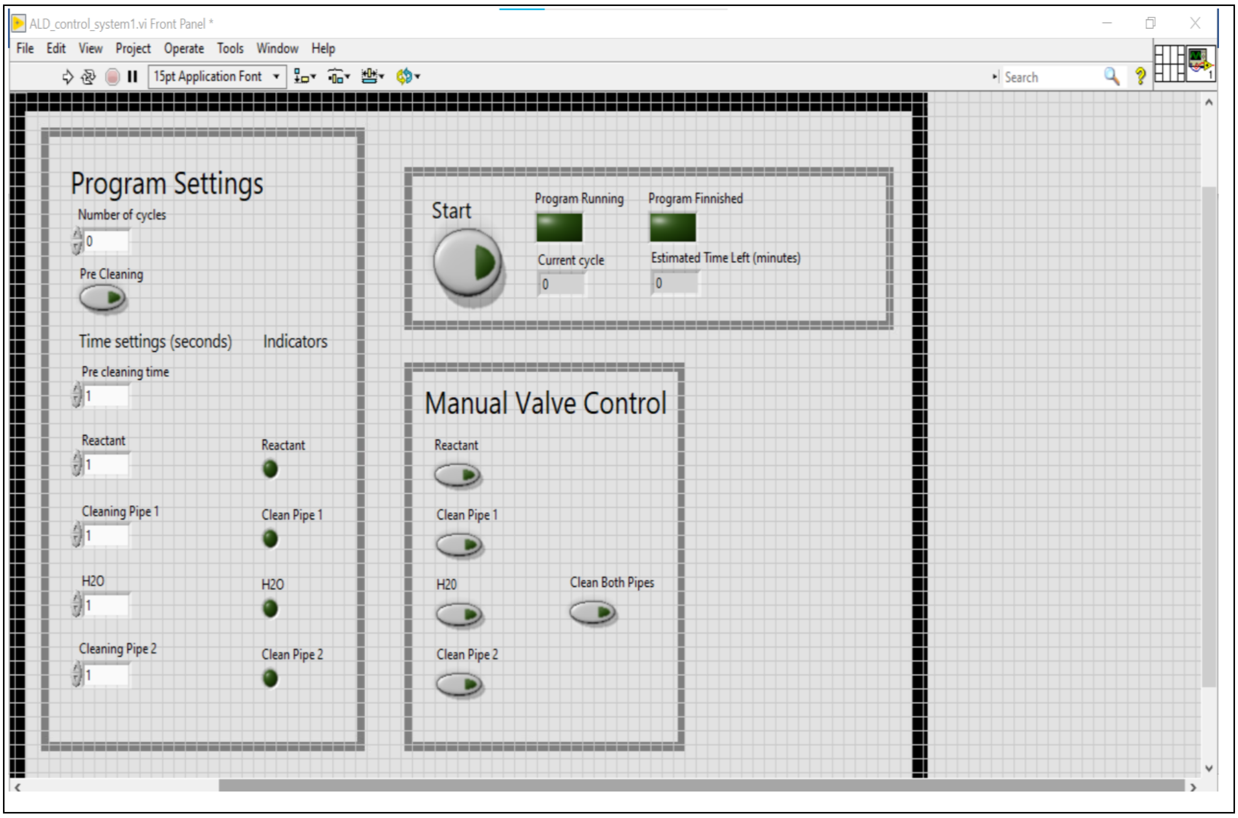

Figure 14. LabVIEW control code graphical user interface - front panel display

In LabVIEW, a graphical user interface (GUI) is built using a set of tools and objects. The user interface is known as the front panel. Code can be added using graphical representations of functions to control the front panel objects. The block diagram shown in Fig. 13 contains this code. Users interact with the front panel when the program is running. There is control of the program, changing inputs, and seeing data updated in real time. Controls are used for inputs such as adjusting precursor pulse and purge times, starting, or stopping a program. Indicators are used as outputs. Indicators display outputs from the program. These may include which ALD cycle number is running, which valve is open and other information.

Every front panel control or indicator has a corresponding terminal on the block diagram. When a VI is run, values from controls flow through the block diagram, where they are used in the functions on the diagram, and the results are passed into other functions or indicators through wires. Users can access controls and indicators by right clicking the front panel.

This program can be run, program settings inputted by typing in the required process specifications and clicking on the relevant buttons as explained in Appendix E (LABVIEW CODE MANUAL). This includes the number of cycles that the program must run, time for each valve to be open/ closed, dose time and pipe cleaning (purging) time for relevant precursor/reactant.

4. EXPERIMENTAL DETAILS

The capability of the ALD reactor operation was tested, demonstrated, and verified by depositing the following oxide thin films: In_2O_3 using an indium triazenide complex as the metal precursor, water vapor as the oxygen source and N_2 was used as the carrier-and-purging gas.

The scope of this work was to develop and then optimize a new ALD process with the homoleptic precursor tris(1,3-diisopropyltriazenide)indium(III) and water for the formation of In_2O_3 thin films.

In this present ALD work, the effects of substrate temperature, process optimization, and reactor tunability on deposited In_2O_3 films using the new indium triazenide precursor have been studied. The important structural, morphological, and optical characterizations: X-ray diffraction (XRD), X-ray reflectivity (XRR), Scanning electron microscope (SEM), X-ray photoelectron spectroscopy (XPS), Ultraviolet-Visible light (UV-Vis) spectrophotometry, Four-point probe on deposited In_2O_3 films were studied, and the optimum parameters were established.

4.1 Film deposition

The homemade ALD system was used to grow metal oxide films. N_2 was used as a carrier-and-purge gas. The growth of In_2O_3 films was performed on Si(100) substrates by alternating reactions of the indium triazenide complex and H_2O. The Si substrates, cut to size, were first cleaned to remove native oxide layers. They were blown free of particles with dry N_2 gas before they were loaded in the ALD reactor heating chamber. After loading the substrates, the chamber was baked at 154 °C overnight.

The heating chamber was first calibrated to determine the actual deposition temperature that the substrate was subjected to in comparison with the one shown on the screen. This was done by using a thermocouple inserted into the chamber, onto the substrate and the temperature measurement was done under actual deposition conditions i.e. low pressure and in carrier gas, N_2 flow.

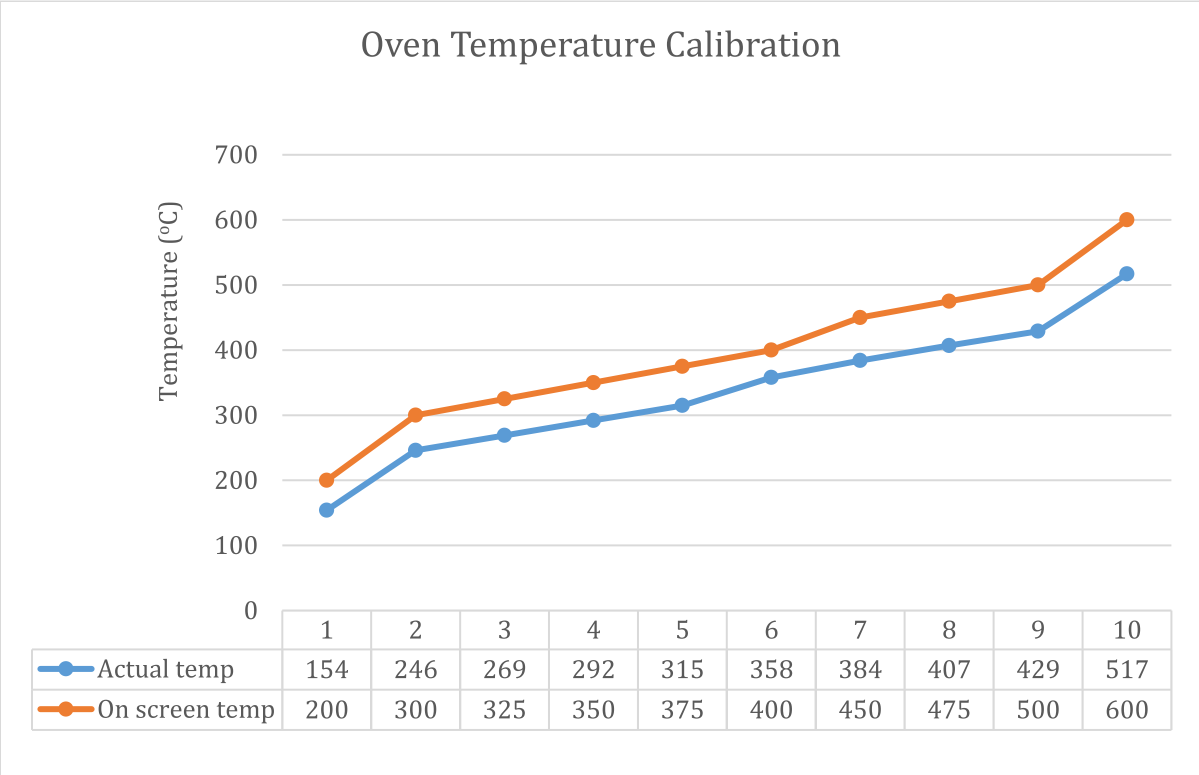

Figure 15. Calibration curves showing the actual vs on-the-screen temperature using a thermocouple.

Precursors and nitrogen gas were introduced into the reactor through gas pipes on the entrance or inlet end of the tube. Unreacted precursors and reaction by-products were removed through the opposite end (exhaust) of the reactor with a vacuum pump. Substrates were also introduced into and removed from the reactor via the removable flange at the exhaust end of the reactor. The deposition zone of the reactor was defined by the heated zone of the tube furnace. Both precursors were introduced sequentially into the reactor at the beginning of this heated zone. The indium triazenide precursor used was invented and synthesized locally at Linköping University.

Indium triazenide precursor delivery lines were heated to a temperature such that the precursor attained a vapor pressure enough for the process to take place. The bubbler containing the solid Indium precursor was heated to 120 °C to develop adequate vapor pressure, while the delivery lines were heated to 140 °C to prevent condensation of the precursor. N_2 carrier gas (constant flow during the deposition) was directed into the bubbler to assist in the complete emptying of the vapor space. At all times during the deposition, the N_2 flow was kept constant. During a purge, no precursors were introduced into the reactor.

Water vapor was introduced into the reactor by the action of an ALD valve connected to the reactor by a stainless-steel pipe. The deionized H_2O was kept at room temperature and delivered by its own vapor pressure without carrier gas. A single water dose consisted of positioning the ALD valve in the dose state for 3 s and then returning it to the purge state for 10 s again. 10 s of purging was allowed between the introductions of the precursors. Under these conditions, one ALD reaction cycle was defined as one dose of the metal precursor followed by a 10 s purge and then one dose of water followed by another 10s purge. To determine the ALD window, deposition temperature was varied from 154 to 517 °C.

4.2 Film characterization

4.2.1 X-ray Diffraction (XRD)

X-ray diffraction is a structural characterization technique used for phase identification of a crystalline material and provides information on unit cell dimensions. It can also be used to get more information that includes phases present in the sample and quantitative phase analysis, crystal structure, unit cell lattice parameters, average crystallite size of nanocrystalline samples, crystallite micro strain, texture, and residual stress.

The principle of XRD is based on constructive interference of monochromatic X-rays on a crystalline sample. These X-rays are generated by a cathode ray tube, filtered to produce monochromatic radiation, collimated to concentrate, and then directed towards the sample. As a result of the interaction between the incident rays and the sample, constructive interference occurs. This relationship is summarized as the Bragg's law:

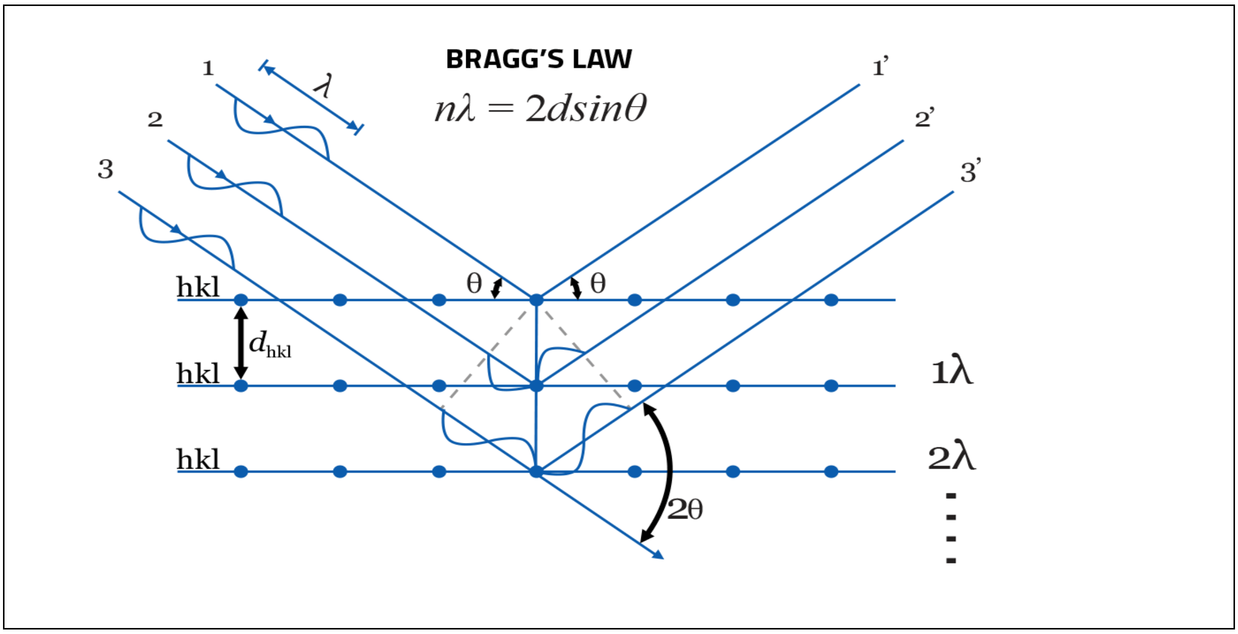

Figure 16. Bragg's Law [65]

where n is an integer, λ is the wavelength of the X-rays, d is the interatomic spacing of the layers and θ is the diffraction angle in degrees.

By changing the diffraction angle, Bragg's Law conditions are satisfied by different d-spacings in polycrystalline materials. Plotting the angular positions and intensities of the resultant diffracted peaks of radiation produces a pattern, which is characteristic of the sample.

Crystallographic phases of the In_2O_3 films were characterized by an X-ray diffractometer PANalytical X'pert Pro, shown in Fig. 17, equipped with a Cu Kα X-ray source (λ=1.54 Å) in the θ-2θ mode, and the scanning angle was changed between 2θ=20° to 90° configuration to minimize peaks originating from the Si(100) substrate. The K_β radiation of the utilized copper source was filtered by a thin nickel foil.

Figure 17. PANalytical X'pert Pro X-ray diffractometer used in this thesis to determine the crystal structure of In_2O_3.

4.2.2 X-ray reflectivity (XRR)

X-ray reflectivity is an analytical technique for investigating thin films, surfaces and interfaces using the effect of total external reflection of X-rays. Reflectivity can be used to characterize single and multilayer structures and coatings in magnetic, semiconducting, and optical materials, among others. Sample thicknesses can be measured using the same X-ray diffractometer shown earlier in Fig. 17 but when switched to XRR mode.

In reflectivity analysis, the X-ray reflection of a sample is measured around the critical angle. At angles below the critical angle of total external reflection, X-rays penetrate only a few nanometers into the sample. Above this angle the penetration depth increases quickly.[66] At every interface where the electron density changes, a part of the X-ray beam is reflected, and the interference of these partially reflected X-ray beams creates an oscillation pattern which gives thickness, density, and roughness.[67]

Based on the reflectivity curves, layer parameters such as thickness and density, interface and surface roughness can be determined, regardless of the crystallinity of the material (single crystal, polycrystalline or amorphous). From the XRR measurements, thicknesses were modeled using the X'Pert Reflectivity software to fit the data using a two-layer model, In_2O_3/Si.

4.2.3 Scanning electron microscopy (SEM)

In scanning electron microscopy, a focused beam of high-energy electrons generates different signals that derive from electron-sample interactions at the sample surface. These signals include secondary electrons (that produce SEM images, mainly used for morphology and topography studies), backscattered electrons (for rapid phase discrimination due to composition contrast), diffracted backscattered electrons (used to determine crystal structures and orientations), X-ray photons (characteristic X-rays that are used for elemental analysis), visible light (cathodoluminescence), and heat. There are some similarities with the usual optical microscope, but SEM has many advantages over the optical microscopes, e.g., large depth of field and much higher resolution. In addition, because the SEM uses electromagnets rather than lenses, one has much better control in imaging parameters such as focus, magnification, and astigmatism, which all affect the final image quality.

In_2O_3 film morphology was analyzed by SEM using a LEO 1550 scanning electron microscope with an acceleration energy of 2 kV. The SEM was also used for film thickness measurements on samples that were too thick or had surface roughness that made XRR measurements difficult. All shown micrographs were recorded using the in-lens detector of the column at a working distance of 3-6 mm.

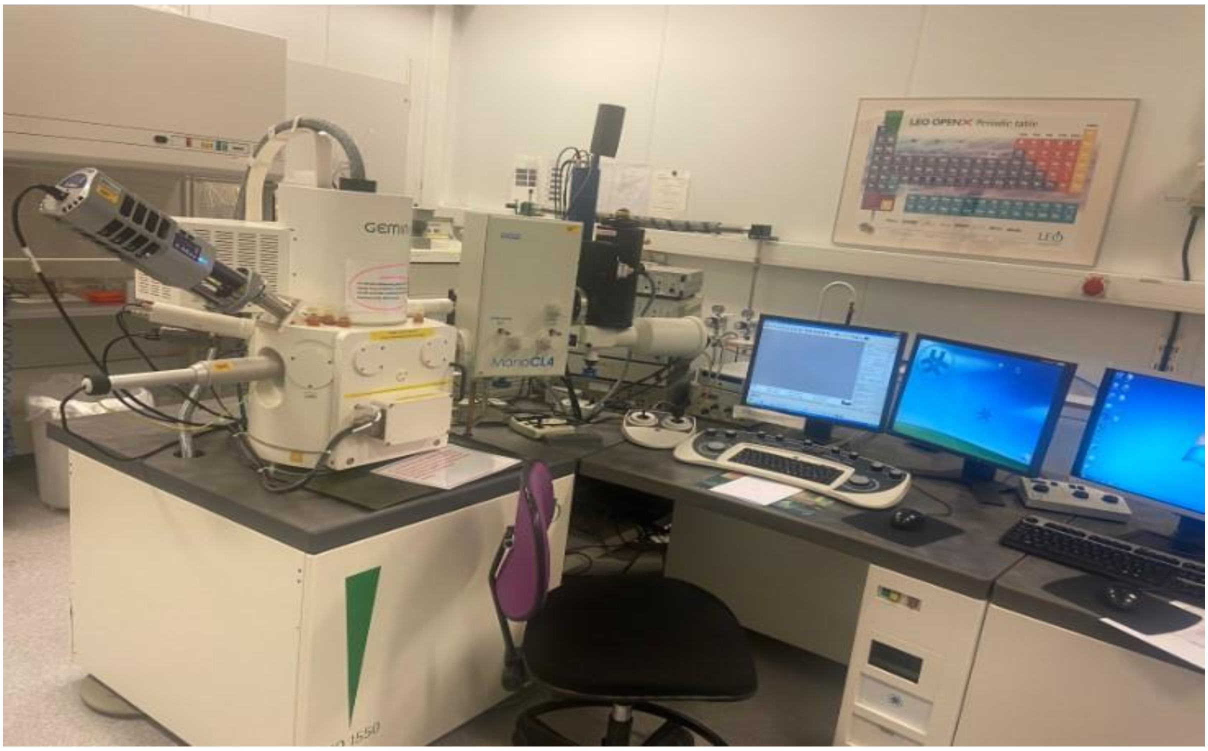

Figure 18. LEO 1550 scanning electron microscope used in this thesis.

4.2.4 X-ray photoelectron spectroscopy (XPS)

X-ray photoelectron spectroscopy is a widely used analytical technique for investigation of chemical composition of thin films. In addition, several other significant thin film materials information can be obtained using XPS, such as chemical states, spatial distribution in three dimensions, film thickness and uniformity.

An XPS system comprises the sample under investigation, primary radiation source and an electron energy analyzer, which are generally kept under ultra-high vacuum. Analysis is accomplished by irradiating a sample with mono-energetic, soft X-rays and then analyzing the energy of the emitted electrons. Photons interact with the atoms at the surface of the sample by photoelectric effect, which causes the surface electrons to be emitted. Binding energies of the emitted electrons are given by the Einstein equation of photoelectric effect:

$E_B = h\nu - E_K - W$

where $h\nu$ is the photon energy, E_K is the kinetic energy of the electron, and W is the spectrometer's work function. Using XPS, E_K is measured by the spectrometer, but is dependent on the photon energy of the X-rays employed. Since all quantities, except the binding energy (E_B), are either known or measurable, it becomes easy to calculate the binding energy of the electron. The binding energy calculation is performed by control electronics associated with the spectrometer.

The elemental composition and possible impurity levels of deposited In_2O_3 films was probed with high resolution XPS, Kratos AXIS Ultra DLD, equipped with an Ar (0.30 eV) sputtering source for 600 s, employing monochromatic Al Kα radiation (hν=1486.6 eV). Sputter-cleaning (sputter-etching) was done to eliminate surface contamination resulting from sample air exposure on the films.

Analysis of the photoelectron spectra was done using the CasaXPS software package (www.casaxps.com). By quantitative analysis, the signals originating from the substrate and the thin film could be de-convoluted and information about the chemical composition of the deposited film could be obtained. Gaussian-Laurentius functions and Shirley background were used to fit the experimental XPS data.

Figure 19. Kratos AXIS Ultra DLD X-ray photoelectron spectroscope used for elemental composition.

4.2.5 Ultraviolet-visible (UV-Vis) spectrophotometry

UV-Vis spectrophotometry is used to determine the absorption or transmission spectra in the UV-Vis region of the electromagnetic spectrum. This means that it uses light in the visible and adjacent (near-UV and near-infrared) ranges. Light absorption of UV and Vis light occurs due to absorption of incident photon energy by electrons which can be excited (such as π-electrons). Optical properties can be determined with the help of Beer-Lambert law, which correlates the intensity of absorption of UV-Vis radiation to the amount of substance present in a sample:

$A = \varepsilon l c$

where A is absorbance, ε is the molar absorption coefficient, l is the path length of a sample and c is the concentration of the compound.

Optical properties of films deposited on glass substrates were studied by this technique. The measurements were done using the Shimadzu UV-2450 UV-Vis spectrophotometer in a wavelength range of 250–800 nm. Absorbance and transmission vs. wavelength graphs were obtained in the mentioned wavelength range.

Figure 20. Shimadzu UV-2450 UV-Vis spectrophotometer used for optical transparency and later band gap determination.

4.2.6 Four-point probe

A four-point probe is used to measure the sheet resistance of a thin material layer in units of ohms per square (Ω/□) by forcing current through two outer probes and reading the voltage across the two inner probes. Using this four-terminal configuration avoids measurement error due to the contact resistance between the probe and sample. If the thickness of a thin film is known, the sheet resistance measured by four-point probe can be used to calculate the resistivity of the material. Conversely, if the material's resistivity is known, the thickness of the thin film can be calculated.

The resistivity is given by:

ρ = (differential voltage x correction factor x thickness of the film) / current injected.

= sheet resistance x correction factor x thickness of film.

Electrical characterization of the films was done by resistivity calculations using this technique performed with measurements done on a Jandel, Model RM3000 test unit or probing system. The probe was first calibrated using a standard glass sample before sheet resistances were read out and respective sample resistivities were determined.

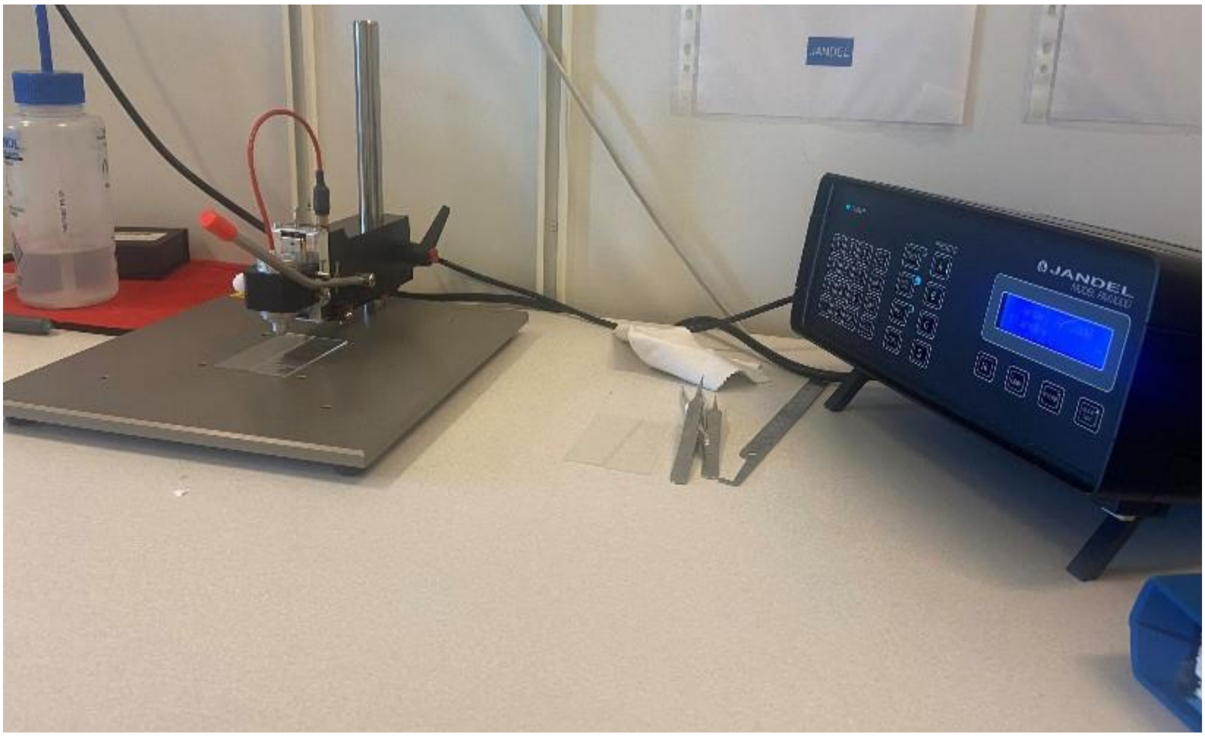

Figure 21. Jandel, Model RM3000 4-point probing system

4.2.7 Tauc plot

A Tauc plot is one of the methods used in determining the optical band gap in semiconducting materials. The square of the product of the absorption coefficient and photon energy is plotted versus photon energy. The curve should have a section that makes a straight line. If extended to the *x*-axis, the *x*-intercept of this line gives the value of the optical band gap.

The optical band gap (E_g) can be calculated from UV-Vis spectrophotometry data, based on the Tauc relation:

$(\alpha h\upsilon)^{1/y} = \beta(h\nu - E_g)$

where α is the absorption coefficient (absorbance/film thickness), h is the Plank's constant, ν is the frequency of incident light, β is the band tailing parameter, E_g is the energy of the optical band gap and y is the power factor which depends upon the nature of the transition (semi-conducting materials, y=0.5 for direct allowed transitions).

By drawing a tangential line from the plotted graph of $h\nu$ versus $(\alpha h\nu)^2$, the value of the band gap is determined as the value of $h\nu$ at the point where this line crosses the axis i.e., the intercept of the extrapolation to near zero absorption with photon energy axis i.e. $(\alpha h\nu)^2 \rightarrow 0$.

In this work, determination of the optical band gap was done using the Tauc plot formalism from absorbance and transmission data obtained from the UV-Vis spectrophotometer mentioned earlier.

5. RESULTS AND DISCUSSION

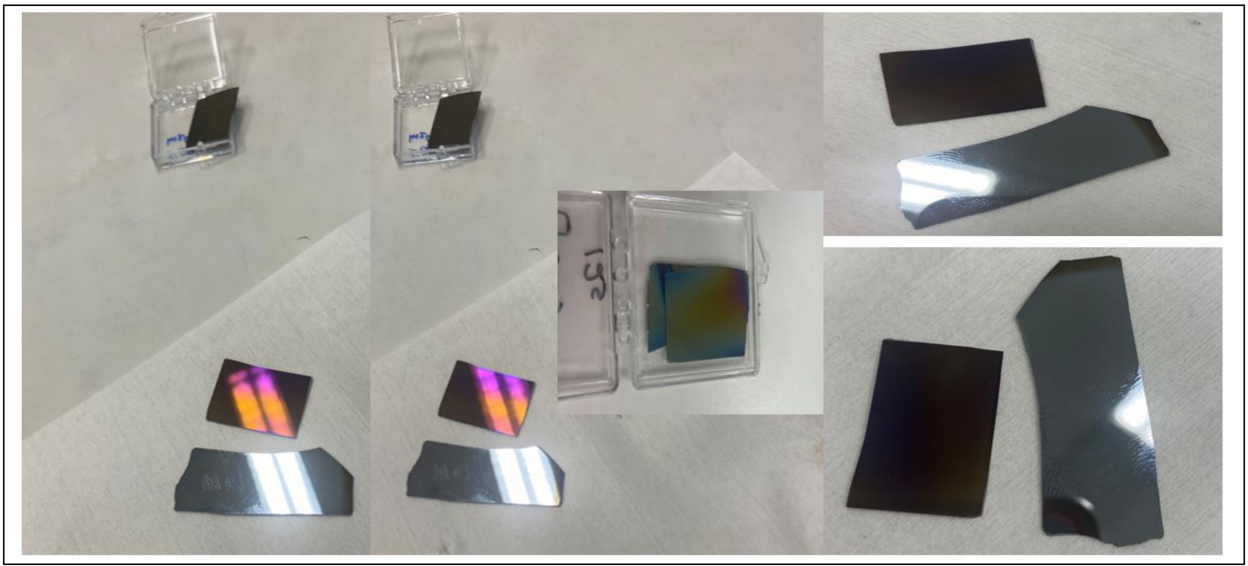

Figure 22. Pictures showing ALD In_2O_3 films on silicon substrates.

5.1 In_2O_3 Growth

Film growth is based on ligand-exchange reaction mechanisms involving breaking the metal-ligand (M-L) bonds of the precursor and an O-H bond on the substrate surface, forming an M-O bond and a L-H bond.

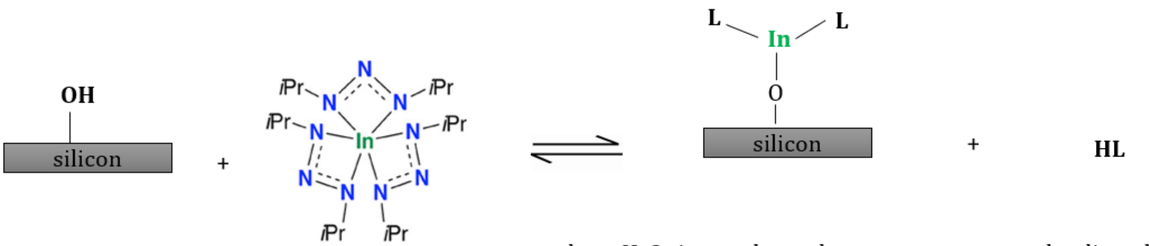

Where the indium ligand, **L** =

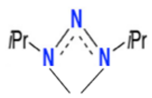

when H_2O is used as the oxygen source, the ligand exchange reaction is envisioned to take place and is the most plausible surface chemical reaction expected - between the ligands of the metal precursor and the silicon substrate surface hydroxyl groups.

This reaction results in formation of new chemical bonds between indium atoms and oxygen atoms as well as the release of protonated ligands as by-products.

The ligand exchange reactions can occur during both the indium precursor pulse and the H_2O pulse.

Figure 23. Schematic of a ligand exchange reaction for the indium triazenide/ H_2O process

The ALD process optimization and the growth characteristics needed for self-limiting growth of films were studied by varying the indium precursor and water oxidant pulse lengths, purge time, deposition temperature and number of deposition cycles. The precursor bubbler temperature was kept constant at just below 120 ^{0}C.

5.1.1 Saturation and growth behavior

With increasing precursor pulse duration to 3 s, the film thickness increased to 50 nm which is a growth rate 1 Å/cycle; no further significant increase in the growth rate was observed for longer precursor pulse durations beyond these 3 s as shown in Fig. 24. The same was done for water pulse duration as illustrated in Fig. 25. Film growth rate was relatively insensitive to changes in water pulse time tested from 3 s to 9 s. This confirms the characteristic self-limiting growth behavior of ALD.

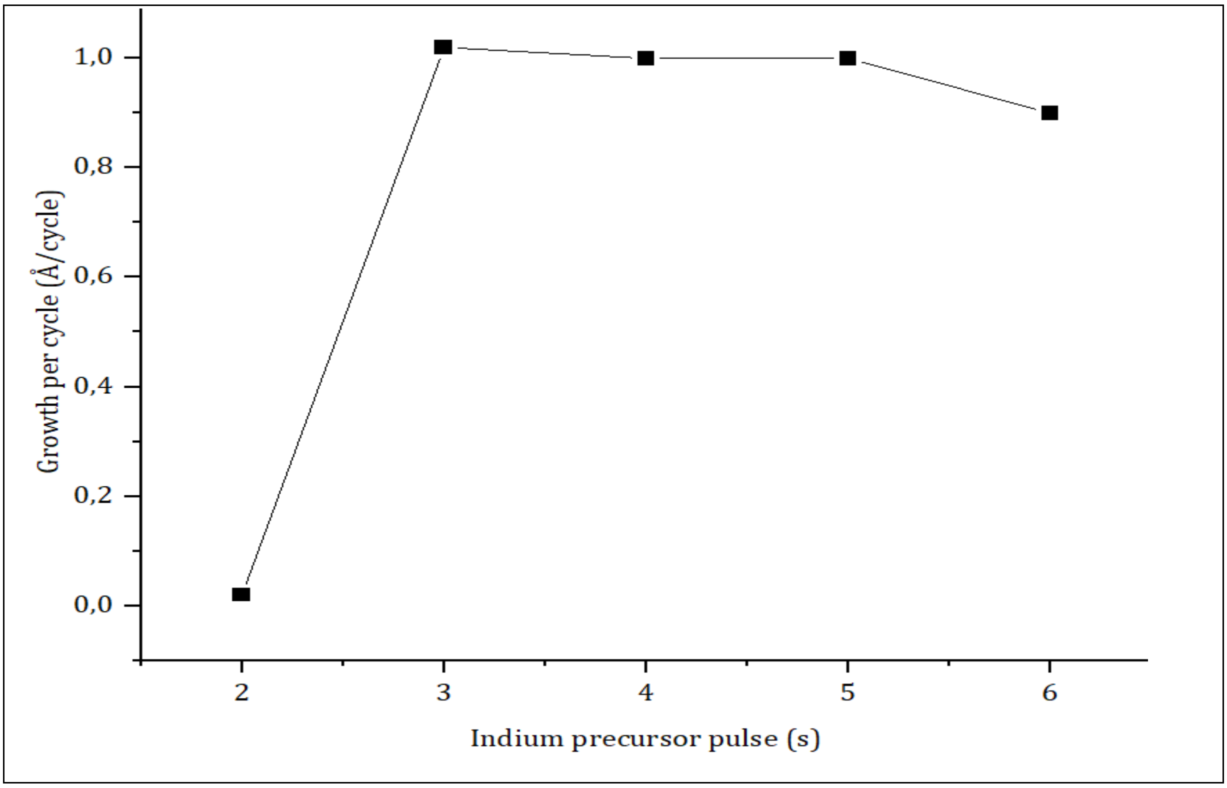

Figure 24. The saturation behavior showing variation of the thickness of In_2O_3 films as a function of Indium precursor pulse length.

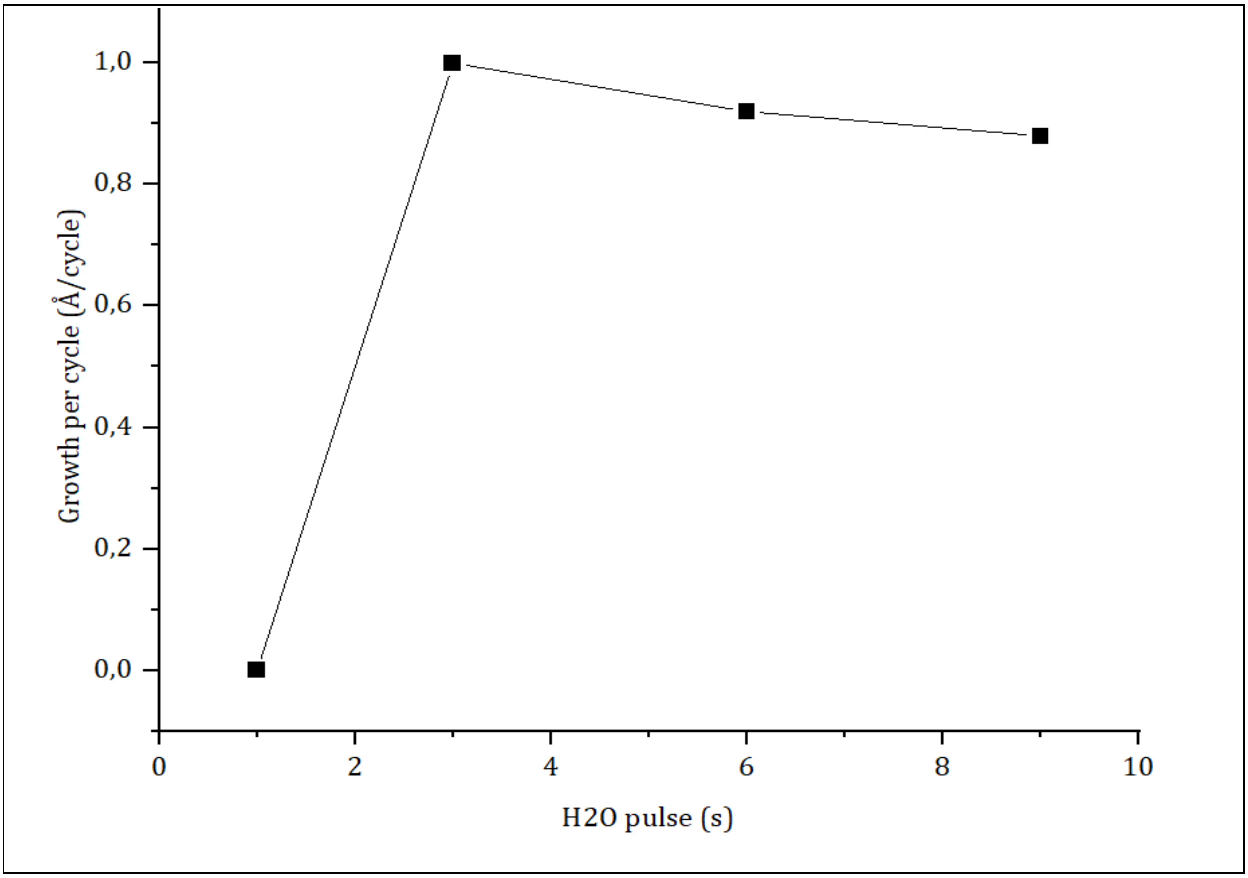

Figure 25. The variation of the thickness of In_2O_3 films as a function of H_2O pulse length.

5.1.2 Film thickness vs. number of cycles

Samples were then deposited at a growth temperature of 292 °C using 300, 500, and 1100 cycles. Fig. 26 shows the film thickness results as a function of the completed number of cycles. An expected linear relation is observed between thickness and number of cycles indicating homogenous growth and linearity effect of the number of cycles on the film thickness. A linear fitting yields a growth rate of ~1 Å/cycle of the film (0.08927 nm = 0.8927 Å) and a nucleation delay of approximately 49 cycles.

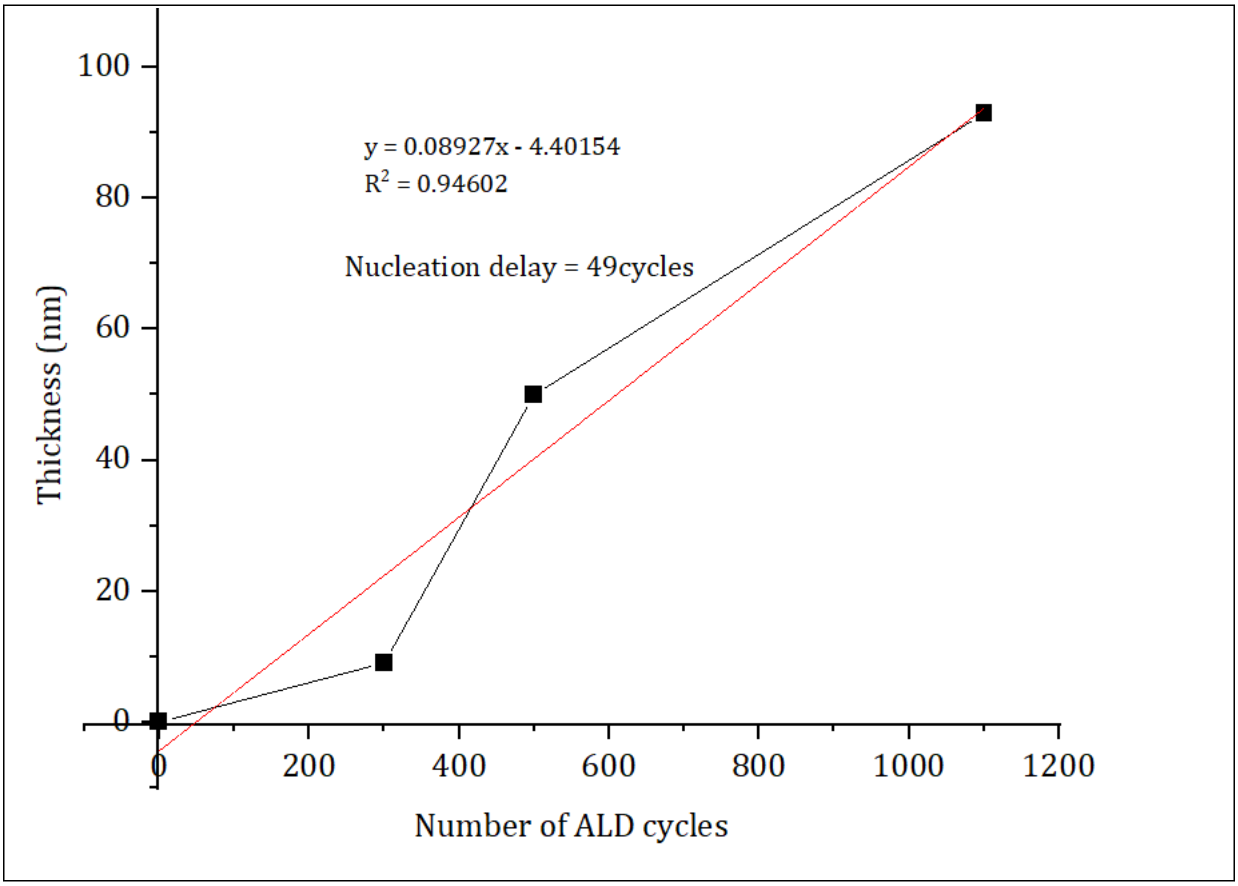

Figure 26. The variation of In_2O_3 film thickness with the number of ALD cycles.

Good linearity demonstrates the thickness tunability with this reactor.

5.1.3 ALD Window

To determine the ALD window and the effect of deposition temperature on the film growth, In_2O_3 films were deposited at various temperatures from 246 ^{0}C to 517 ^{0}C. The In_2O_3 film growth rate dependence on reactor deposition temperature is shown in the graph of growth rates of at various deposition temperatures in Fig. 27. It is found to be independent of reactor temperature between 269 ^{0}C and 384 ^{0}C, indicating adsorption-controlled growth regime.

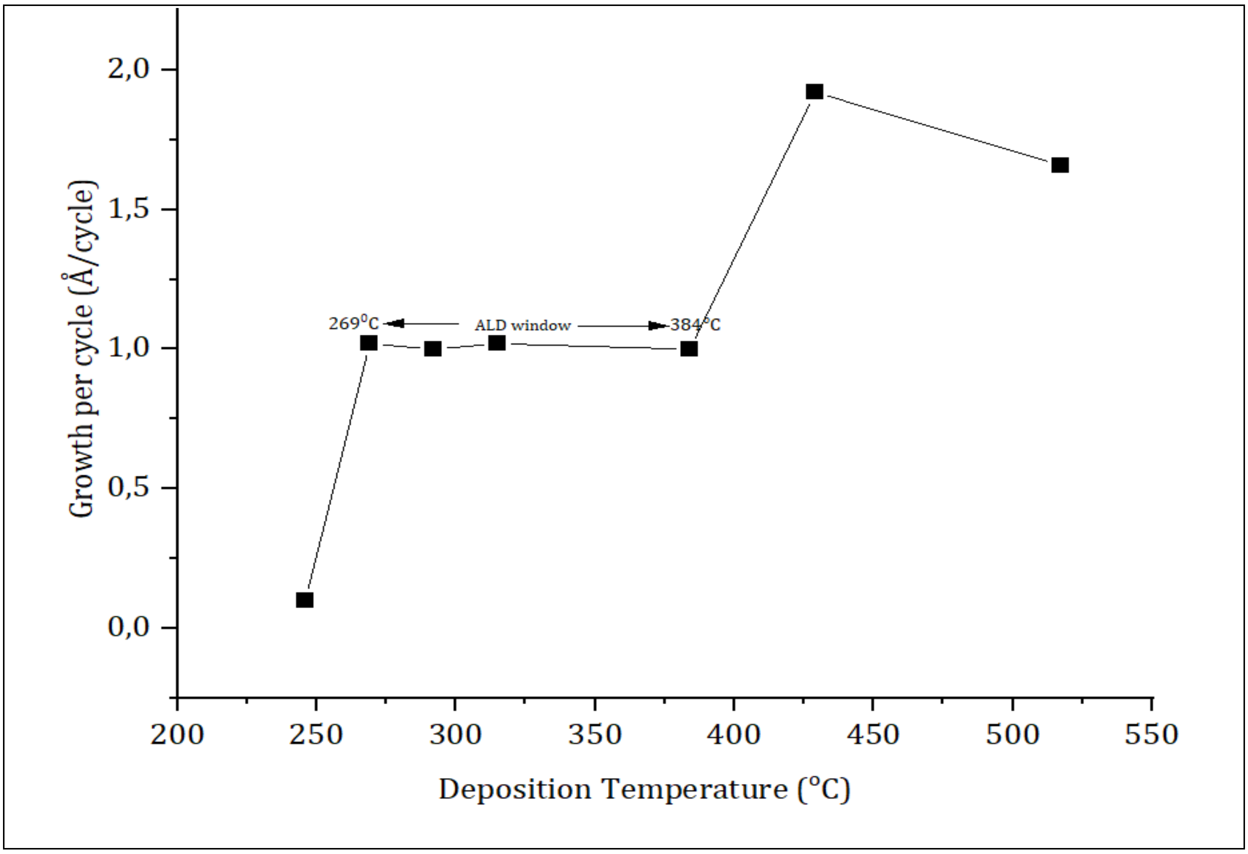

Figure 27. The growth rates of In_2O_3 ALD at various deposition temperatures to determine the ALD window.

SEM was used for film thickness measurements on two samples grown at 429 ^{0}C and 517 ^{0}C because they were too thick to be measured by XRR hence their thickness values are not extremely accurate but very much indicative of how very thick the films are.

5.2 In_2O_3 Properties

5.2.1 Elemental composition

Table 3. Elemental percentages of In_2O_3 films deposited at different temperatures (at oxidant pulse time of 3s) and different oxidant dosages (at temperature 292^0C).

Deposition temperature	C	In	O	Atomic ratio In:O (Expected 1:1.50)
292^0C	3.50%	43.55%	52.95%	1:1.22
315^0C	1.43%	44.95%	53.62%	1:1.19
384^0C	0%	51.5%	48.5%	1:0.94
Oxidant pulse length				
3s	4.33%	43.19%	52.47%	1:1.21
6s	1.3%	45.3%	53.4%	1:1.18
9s	0.8%	45.6%	53.6%	1:1.18
12s	1.3%	44.7%	54.0%	1:1.21

XPS analysis revealed little to no carbon and negligible nitrogen impurity incorporation within the films, e.g., at 315 ^0C where the survey spectrum of the 50 nm-thick film shows an indium rich non-stoichiometric indium oxide i.e. In ~ 45 at. %; O ~ 53 at. % with trace amounts of carbon (~1.4 at. %). From Table 3, it indicates that the higher the deposition temperature and oxidant dosage time, the less the impurity of C in the deposited In_2O_3 film. Even though XPS has confirmed the oxygen deficient nature of the deposited In_2O_3 films, an increase in oxidant dosage times also helps to increase the O content and reduce the impurity content of the films. Therefore, a conclusion can be drawn that contamination-free In_2O_3 films can be deposited using this indium precursor with relatively high growth rates.

It is also important to note that the deposited films exhibit an average In:O ratio of 1:1.20 with negligible carbon, which is below the stochiometric 1:1.50 ratio. This reveals the possibility of existence of oxygen vacancies in the In_2O_3 films. Oxygen vacancies, created when bonds are weakened, are essentially point 'defects' in metal oxides that are incorporated into the film crystal structure during the deposition process. These oxygen vacancies are critical in explaining the optoelectrical properties of metal oxide thin films.

5.2.2 Crystallinity

The crystallinity of the In_2O_3 ALD films, investigated using XRD, 2θ scans from 20° to 90° were determined on about 50 nm thick In_2O_3 films deposited on Si substrates at different temperatures. Crystallinity was examined at different growth temperatures: 315^{0}C and 429 ^{0}C. The diffraction patterns show that the In_2O_3 films deposited were polycrystalline in nature with a cubic phase. The crystalline peaks in the XRD spectrum well matched with the diffraction data of cubic indium oxide from the X'Pert HighScore Plus software.

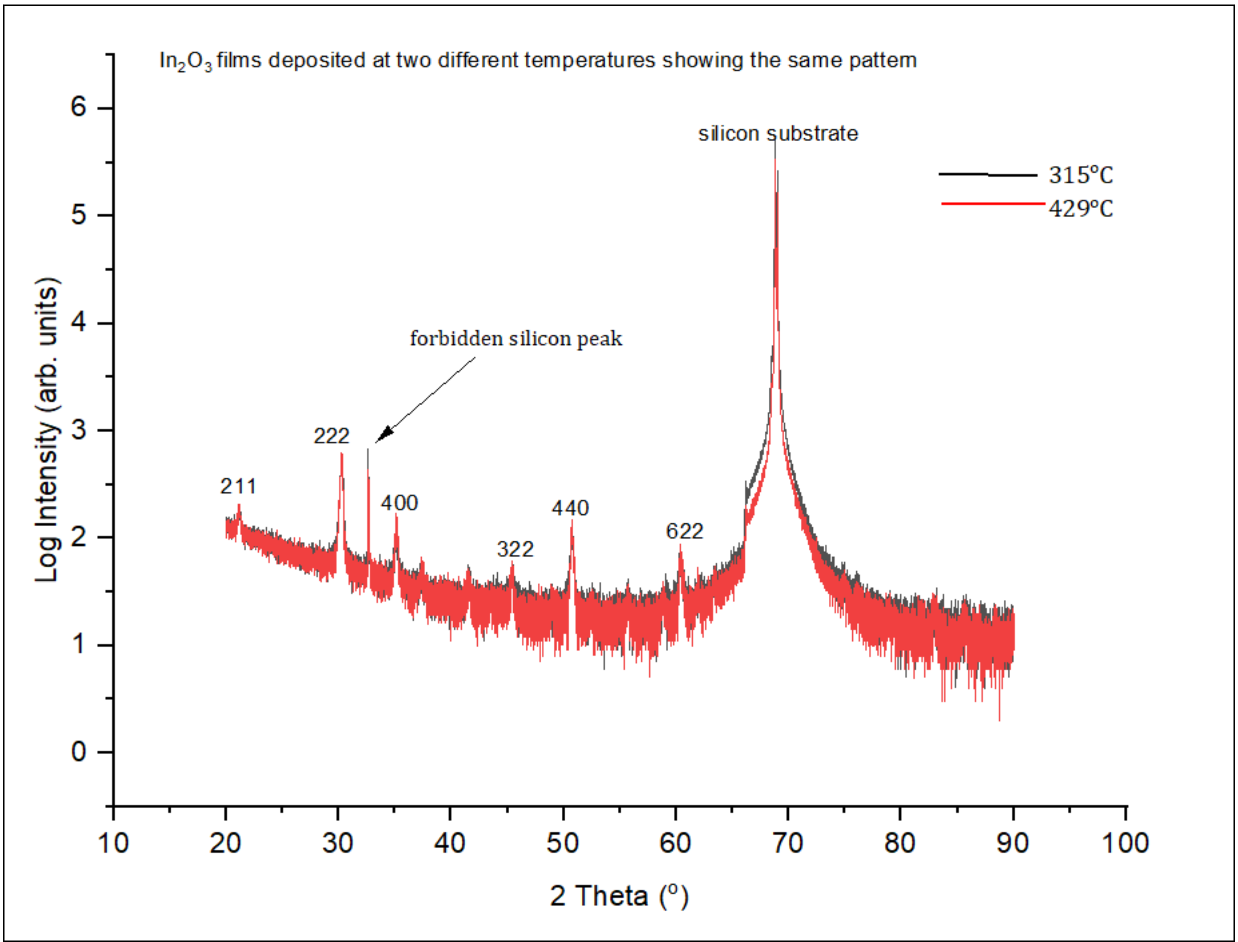

Figure 28. XRD spectra of In_2O_3 films confirming polycrystalline structure.

At these two temperatures, the diffraction peaks indicated the growth of polycrystalline In_2O_3 films with cubic structures, as earlier mentioned, (211) at 21^0, (222) at 30^0, (400) at 35^0, (332) at 42^0, (440) at 51^0 and (622) at 60^0, with (222) having the highest intensity.

5.2.3 Surface morphology

The SEM images show the morphology of the films deposited at temperatures 292 ^{0}C, 315 ^{0}C, 429 ^{0}C and 517 ^{0}C. At lower deposition temperatures that are within the ALD window (292 ^{0}C and 315 ^{0}C), the films are quite smooth as illustrated in Fig. 29a) and b). Then at an increased temperature of 429 ^{0}C, Fig. 29c), the grains became flattened, faceted, and densely arranged with no visible pinholes, giving smooth films as well.

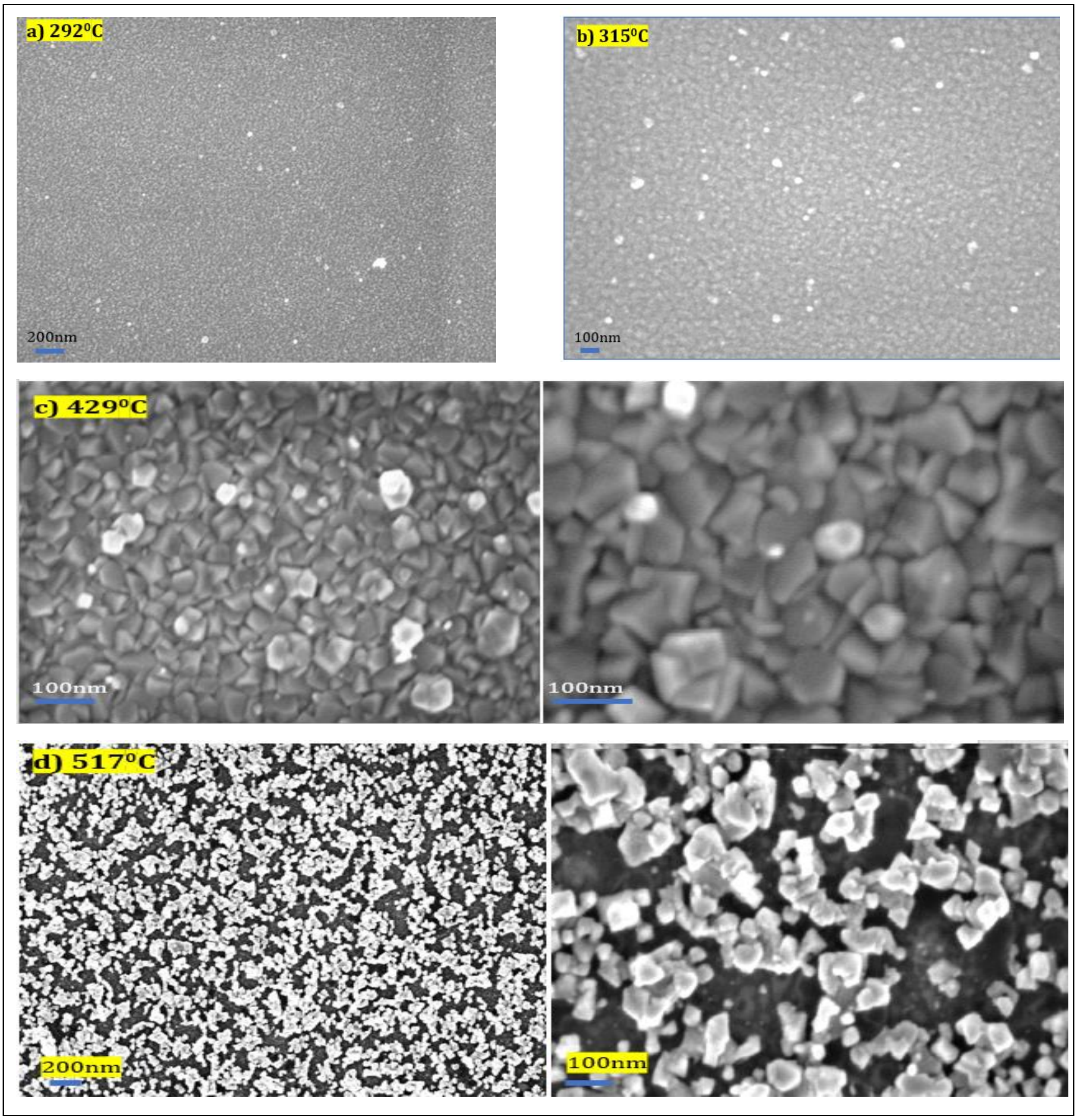

Figure 29. SEM images for the films deposited within the ALD window at 292 ^{0}C (a) and 315 ^{0}C (b), outside the ALD window at 429 ^{0}C (c) and 517 ^{0}C (d)

Films deposited at a further increased temperature 517 ^{0}C showed a rather strange morphology different from the morphology observed at lower temperatures. Its grains were randomly arranged with some voids or pores as displayed in Fig. 29d). This is a suspected result of roughness from decomposition of the indium precursor. The film showed a rather roughened surface morphology with more pronounced grains compared to the rest.

From the topographical overview of some parts of most samples' top surfaces, several very small particles, or grains like are seen, which could just be a sign of edge contrast.

Growth of smooth, uniform, and thick In_2O_3 films was also verified and confirmed using cross-sectional SEM analysis as illustrated in Fig. 30.

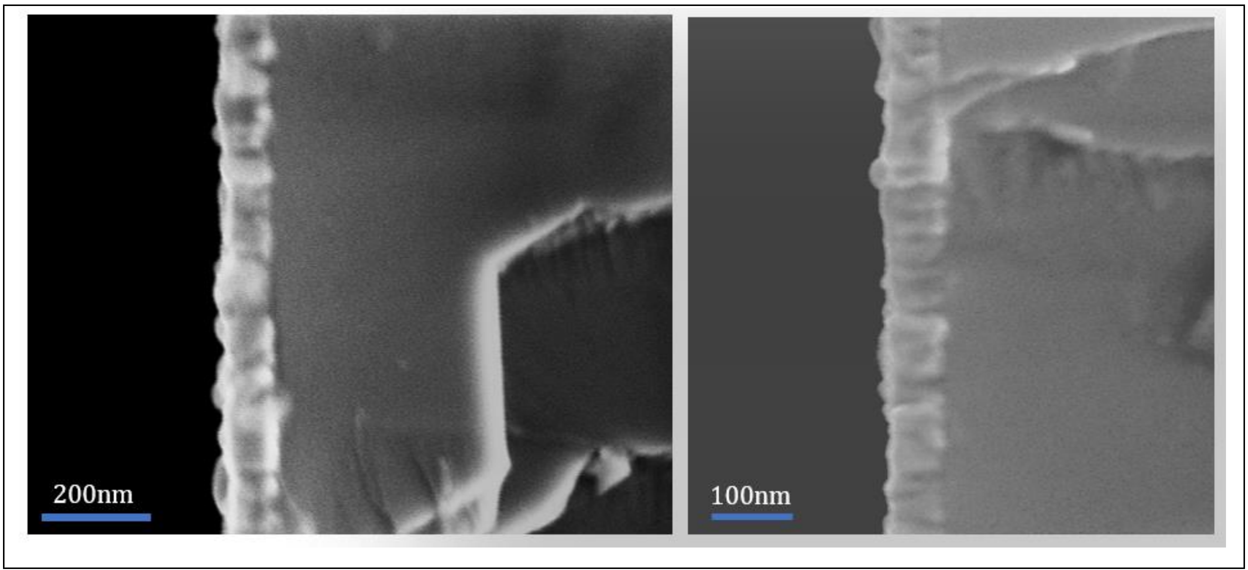

Figure 30. Cross-sectional SEM images confirming the growth of smooth and uniform thin films using this ALD process.

5.2.4 Resistivity

Electrical characterization through resistivity of the In_2O_3 films was determined by four-point probe measurements done on approximately 51 nm thick In_2O_3 films deposited on glass at the same temperature (292 ^{0}C), but with supposedly different oxygen quantities. Film resistivity is a true reflection of the electrical properties of a film since it is determined by the carrier concentration and mobility.

Electrical conductivity of films is mainly controlled by the oxygen stoichiometry in the film. A perfect In_2O_3 stoichiometry is not ideal since it has fewer oxygen vacancies which results in increased resistivity. So In_2O_3 exhibits n-type semiconducting properties which arise due to oxygen vacancies within the lattice that can act as donors not acceptors.

The films show a general decrease in resistivity (increase in conductivity) with increasing oxidant dosage. The improved conductivity for films deposited with increased H_2O dosage may also be attributed to incorporation of hydroxyl groups which cause self-doping.[68]

Another obvious possibility is the presence of In–In metal bonds in the films that are likely to provide fast conduction paths for the electrons hence resulting in low resistivity values.

The resistivities of different film samples, all with 51 nm thicknesses, deposited at 6 s, 9 s and 12 s of water pulse were 1.22, 2.58 and 0.16 mΩcm, respectively.

Table 4. Resistivities of In_2O_3 films grown at different oxidant doses, all 51nm thick.

H_2O pulse (s)	**Sheet Resistance 1** (Ω/□)	**Sheet Resistance 2** (Ω/□)	**Sheet Resistance 3** (Ω/□)	**Average** (Ω/□)	**Resistivity** (Ω.cm)
6	242,11	233,02	241,26	238,80	1,22E-03
9	526,69	494,85	498,7	506,75	2,58E-03
12	32,61	31,57	32,53	32,24	1,64E-04

5.2.5 Optical transparency

Obtaining an optical transmission spectrum of In_2O_3 films deposited on glass referenced to the spectrum of the uncoated glass substrate, the resultant average transmission of the In_2O_3 film in the wavelength range 250–800 nm was calculated using the relationship:

$$\boxed{A = 2 - \log_{10} (\%T)}$$

where A is absorbance and T is transmittance of visible light.

Optical transmittance for approximately 50 nm thick films deposited at 292 °C on glass using the two precursors is shown on the optical spectrum in Fig. 31 with an uncoated substrate of glass also included for reference.

The highest obtained optical transmittance of 71 % in comparison to an uncoated glass substrate which was found to be 74 % is very much commendable and comparable to the values already reported in literature.[69,70]

Fig. 31 shows that the transmittance increases with oxygen content. It is notably lower for films deposited at lower dose time of the oxidant source. The origin for the notable difference is based on oxygen stoichiometry in the films which has an impact on both optical transmission and electrical conductivity of the films.

When oxygen dosage was higher, the films became more transparent and thus a better transmittance could be achieved. At higher oxygen dosage and content, the transmittance was as high as to be close to that of the uncoated glass substrate, which suggested that the films were getting closer to being stoichiometric. This result was consistent with the previous results as shown in Table 3 for XPS analysis.

Just like in any other metal oxide, even though oxygen vacancies are one of the most common defects, it has become apparent that oxygen vacancies can, in fact, induce new properties as seen with optical transparency. This subject will be discussed further under optical bandgap results.

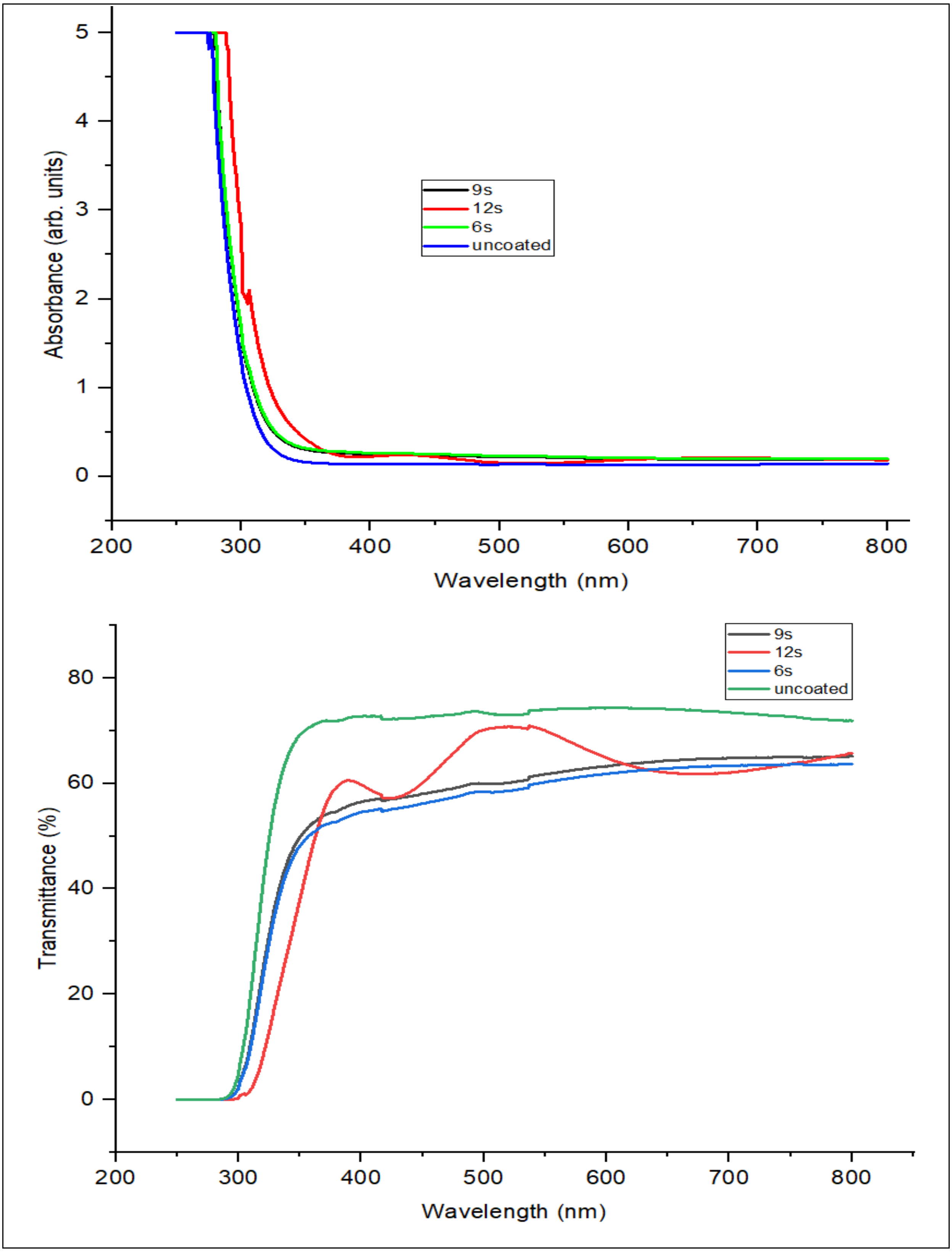

Figure 31. Different absorbances within the visible light range, showing varying optical transmissions at different oxygen contents of the films. This is based on the oxidant (H_2O) dose times of 6 s, 9 s and 12 s. Transmittance is shown to generally increase with increasing oxidant dosage time.

5.2.6 Band gap

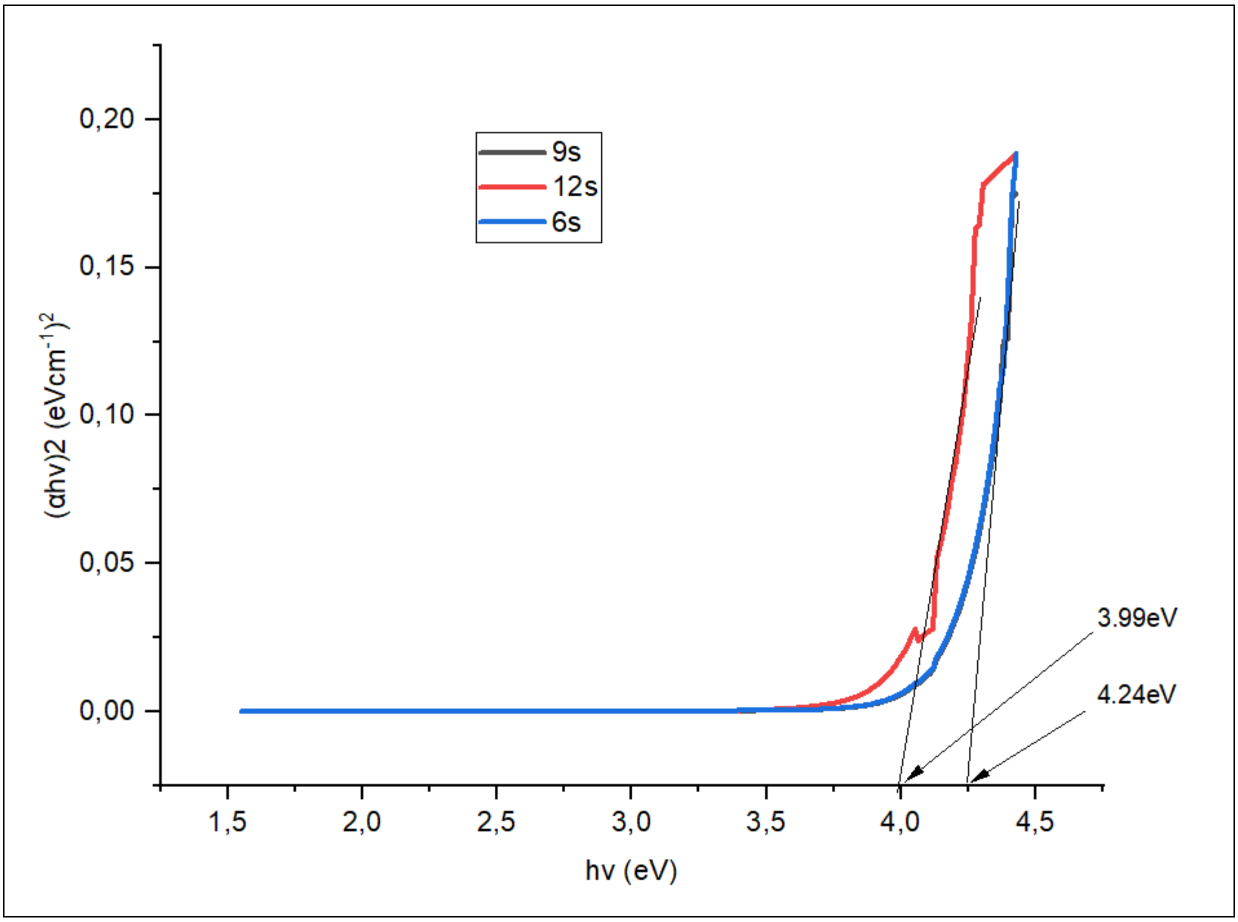

Figure 32. Tauc Plot: Optical band gap spectra from films deposited at different oxygen dosages.

From these curves it is observed that best fit is obtainable for $(\alpha h\nu)^2$ vs. hν (photon energy) which indicates direct allowed transition. The plot of $(\alpha h\nu)^2$ vs. hν of the In_2O_3 films for the different oxidant dosages shown in Fig. 32 shows that the direct optical band gap varies between 3.99 and 4.24 eV. The band gap of In_2O_3, just like its morphology and electrical properties primarily depends on such factors like the temperature, atmosphere, and the nature of the substrate on which the film is to be deposited and these parameters need to be tuned accordingly during the deposition process.[71]

The obtained band gap (3.99-4.24 eV) is comparable to previously reported but is slightly higher than the expected range (3.55-3.85 eV) most likely because our deposition temperatures were higher (292 ^{0}C) than what is normally employed in most ALD studies. As seen from XPS results, higher deposition temperatures cause the reduction of oxygen vacancies and carbon impurities in the deposited film. At the atomic level, oxygen vacancies are simply a representation of the lack of a few ions in a huge matrix of oxide material surrounding them. Oxygen vacancies are electronic states that reside within the bandgap, below the conduction band.

The increase of band gap, despite the reported low resistivity can also be explained by the gap widening phenomenon called the Burstein−Moss shift.[72] The band increases due to the filling up of low-lying energy levels in the conduction band. Hence the shift of adsorption edge towards higher energy due to increased carrier density. However, if there are lots of oxygen vacancies in a metal oxide thin film, impurities states can become more localized and can overlap with the valence band edge narrowing or reducing the band gap.

In addition, high temperatures generally enhance crystallinity, which in turn influences the optical band gap of the In_2O_3 films in a way. This is because as the deposition temperature rises, the grain size of the deposited In_2O_3 film increases, leading to a decrease in the density of grain boundaries in the film. Since electrons are easily trapped in the grain boundaries, the number of free electrons should increase in the In_2O_3 film with less grain boundaries. As a result of such an increased electron concentration, an increased optical band gap is obtained.

6. CONCLUSIONS

6.1 Summary

The goal of this project was to design, build and test a homebuilt reactor for depositing new oxide thin films using ALD. The reactor setup as described was built and successfully tested with ALD of In_2O_3 films using the said novel precursor combinations. A new and promising water assisted In_2O_3 ALD process employing a new triazenide precursor was reported. Notably, studies on deposition and characterization of thin films of indium oxide are of great importance, as this material has the potential to enable various technologies, such as transparent electronics.

Indium triazenide and H_2O vapor generated from de-ionized water were used as the metal and oxygen sources, respectively. The ALD process developed in this work exhibited saturation growth behavior within a 269 ^{0}C – 384 ^{0}C window. Saturation growth is essential in depositing uniform and smooth thin films. This In_2O_3 deposition process also proved the ability of the homebuilt reactor to deposit thick, thin films. To optimally synthesize the films, the substrates were exposed to the metal precursor (for 4 s), purged in the flow of pure nitrogen (for 10 s), exposed to the H_2O vapor (for 3 s), and again purged in the flow of pure nitrogen (for 10 s). The typical growth rate was 0.004 nm/s as the films were deposited on Si substrates.

ALD chemistries were systematically evaluated, and properties of the films obtained from the process thoroughly characterized. The structure of the films was determined by XRD to be cubic and polycrystalline. In addition, a commendable growth rate of 1 Å per cycle was obtained through XRR analysis. The resultant films were analyzed with XPS and found to be sub-stoichiometric In_2O_3 with trace amounts of carbon. ALD rate, film purity and optoelectrical properties are in good agreement with literature values. Most importantly, as transparent conducting oxides with a moderately high transmittance (>70 % in visible light) compared to uncoated glass that had 74 % transmission, an optical band gap ranging between 3.99-4.24 eV and electrically superior properties to most previous studies (low resistivity~0.2 mΩcm), the In_2O_3 films make very good candidates for many potential optoelectronic applications such as photovoltaic devices, liquid crystal displays, transparent conductive electrodes in electronic devices, solar cells and flat panel displays, photodetectors, gas sensors, heat reflecting windows etc.

6.2 Outlook

As a future consideration and a possible follow-up to this study, the effect of composition, electrical mobility, visible light transmission, crystallinity, and morphology as a function of growth parameters on the deposited In_2O_3 films should be studied in detail. For example, the effect of temperature changes on electrical conductivity, optical transparency, and the transition between amorphous and crystalline films.

Saturation, and self-limiting growth behavior of other group 13 oxides besides In_2O_3 from the respective triazenide precursors might be optimized and new processes can be developed. Because an enormous range of desirable properties are being explored for potential applications as functional oxides, we can also go further and deposit ternary compound films, for example indium-gallium-oxide or the famous indium-tin-oxide. Deposition of these oxide thin films, using their respective precursors would be another set of novel and probably better precursor combinations for transparent conducting oxide synthesis.

In addition, quaternary metal-oxide compounds by adding zinc or tin into indium-gallium-oxide can be synthesized, which is another set of promising materials in optoelectronics. Both ternary and quaternary transparent conducting oxide alloys have better properties for transparent and flexible electronics applications, hence a great potential as key materials in the display industry for instance as channel layers in oxide semiconductor thin-film transistors.

REFERENCES

[1] Mato Knez, ALD-A Versatile Tool for Nanostructuring. *Material Matters.* **2008**, 3(2), 28.

[2] H. Zhang, R. Solank, B. Roberds, G. Bai, and I. Banerjee. High permittivity thin film nanolaminates, *Journal of Applied Physics*, **2000**, 87(4):1921 – 1924.

[3] Riddhiman Medhi, Maria D. Marquez, T. Randall Lee. Visible-Light-Active Doped Metal Oxide Nanoparticles: Review of their Synthesis, Properties, and Applications. *ACS Appl. Nano Mater*. **2020**, 3(7) 6156–6185.

[4] Arora A. K, Jaswal V. S, Singh K, Singh R. Applications of Metal/Mixed Metal Oxides as Photocatalyst: A Review. *Orient J Chem,* **2016**; 32(4); 2035–2042.

[5] Michael Lubitz, Phillip A. Medina, IV, Aleks Antic, Joseph T. Rosin, and Bradley D. Fahlman, Cost-Effective Systems for Atomic Layer Deposition, *J. Chem. Educ*. **2014**, 91 (7), 1022–1027.

[6] Fredrik Lundvall, Johan Ottosson, Matilda Andersson, Tobias Broman. Konstruktion av en atomlagerdeponeringsugn - Framtagning av en enkel och kostnadseffektiv atomlagerdeponeringsugn. *Tekniska högskolan vid Linköpings universitet,* TMMI53, **2019.**

[7] Barron, A. R., MOCVD of group III chalcogenides. *Advanced Materials for Optics and Electronics*, **1995**, 5, 245-258.

[8] P. Raghunath, M.C. Lin, Computational study on the mechanisms and energetics of trimethylindium reactions with H_2O and H_2S, *J. Phys. Chem. A*, **2007**, 111, 6481-6488.

[9] Anatolii A. Malygin, Victor E. Drozd, Anatolii A. Malkov, and Vladimir M. Smirnov. From V. B. Aleskovskii's "Framework" Hypothesis to the Method of Molecular Layering/Atomic Layer Deposition, *Chem. Vap. Deposition,* **2015**, 21, 216–240.

[10] A.M. Shevjakov, G.N. Kuznetsova, and V.B. Aleskovskii, Chemistry of High-Temperature Materials, *Proceedings of the Second USSR Conference on High-Temperature Chemistry of Oxides*, Leningrad, **1995.**

[11] S.I. Kol'tsov, V.B. Aleskovskii, Effect of the degree of dehydration of silica gel on the mechanism of hydrolysis of adsorbed titanium tetrachloride, *Russ. J. Phys. Chem*., **1968**, 42 (630), 1210.

[12] S.I. Kol'tsov, Preparation and investigation of products of interaction of titanium tetrachloride with silica gel, *Russ. J. Appl. Chem*., **1969**, 42 (975), 1023-1028.

[13] Suntola Tuomo (02610 Espoo 61, SF), Antson, Jorma (Vantaa 35, SF), Method for producing compound thin films, United States Patent 4058430, **1977.**

[14] H.C.M. Knoops, S.E. Potts, A.A. Bol, and W.M.M. Kessels, Ch. 27 - Atomic Layer Deposition in *Handbook of Crystal Growth*, edited by T. Kuech (Elsevier, **2015**), 1101–1134.

[15] R. L. Puurunen, Surface chemistry of atomic layer deposition: A case study for the trimethylaluminum/water process, *J. Appl. Phys*. **2005**, 97, 121301.

[16] Christophe Detavernier, Jolien Dendooven, Sreeprasanth Pulinthanathu Sree, Karl F. Ludwig, Johan A. Martens. Tailoring nanoporous materials by atomic layer deposition. *Chem. Soc. Rev*., **2011**, 40, 5242–5253.

[17] Marja N. Mullings, Carl Hägglund, Jukka T. Tanskanen, Yesheng Yee, Scott Geyer, Stacey F. Bent. Thin film characterization of zinc tin oxide deposited by thermal atomic layer deposition, *Thin Solid Films*, **2014**, 556, 186-194.

[18] Md. Anower Hossain, Kean Thong Khoo, Xin Cui, Geedhika K Poduval, Tian Zhang, Xiang Li, Wei Min Li, Bram Hoex. Atomic layer deposition enabling higher efficiency solar cells: A review. *Nano Materials Science,* **2020**, 2, 204–226.

[19] K. Wetchakun, T. Samerjai, N. Tamaekong, C. Liewhiran, C. Siriwong, V. Kruefu, A. Wisitsoraat, A. Tuantranont, S. Phanichphant Semiconducting metal oxides as sensors for environmentally hazardous gases. *Sensors and Actuators B: Chemical.* **2011**, 160(1), 580-591.

[20] Chavali, M.S., Nikolova, M.P. Metal oxide nanoparticles and their applications in nanotechnology. *SN Appl. Sci*. **2019**, 1, 607.

[21] Kyung Min Choi, Gun Woo Hyung, Jin Woo Yang, Ja Ryong Koo, Young Kwan Kim, Sang Jik Kwon, Eou Sik Cho. Fabrication of Atomic Layer Deposited Zinc Oxide Thin Film Transistors with Organic Gate Insulator on Flexible Substrate, *Molecular Crystals and Liquid Crystals*, **2010**, 529(1), 131-136.
[22] Y. D. Ko, J. Y. Kim, H. C. Joung, S. H. Ahn, K. S. Jang, Y. J. Lee, J. Yi, Low temperature deposited transparent conductive ITO and IZTO films for flat panel display applications. *J. Ceram. Process. Res.* **2013**, 14, 183.

[23] Nafarizal, N. Precise Control of Metal Oxide Thin Films Deposition in Magnetron Sputtering Plasmas for High Performance Sensing Devices Fabrication. *Procedia Chem.* **2016**, 20, 93–97.

[24] Chuang, K.-T.; Abdullah, H.; Leu, S.-J.; Cheng, K.-B.; Kuo, D.-H.; Chen, H.-C.H.; Chien, J.-H.; Hu, W.-T. Metal oxide composite thin films made by magnetron sputtering for bactericidal application. *J. Photochem. Photobiol. A Chem.* **2017**, 337, 151–164

[25] Snyders, R.; Dauchot, J.-P.; Hecq, M. Synthesis of Metal Oxide Thin Films by Reactive Magnetron Sputtering in Ar/O_2 Mixtures: An Experimental Study of the Chemical Mechanisms. *Plasma Process. Polym*. **2007**, 4, 113-126.

[26] Gil-Rostra, J.; Chaboy, J.; Yubero, F.; Vilajoana, A.; Gonzalez-Elipe, A.R. Colored and Transparent Oxide Thin Films Prepared by Magnetron Sputtering: The Glass Blower Approach. *ACS Appl. Mater. Interfaces* **2013,** 5, 1967–1976.

[27] J. Asbalter, S. Karunakaran and A. Subrahmmanyam, Properties of indium oxide thin films prepared by reactive electron beam evaporation technique for EMI control. *Proceedings of the International Conference on Electromagnetic Interference and Compatibility*, New Delhi, India, **1999**, 366-371.

[28] K S Shamala, L C S Murthy and K Narasimha Rao. Studies on tin oxide films prepared by electron beam evaporation and spray pyrolysis methods. *Bull. Mater. Sci.* **2004**, 27(3), 295–301.

[29] Joni Huotari, Jyrki Lappalainen, Jarkko Puustinen, Tobias Baur, Christine Alépée, Tomi Haapalainen, Samuli Komulainen, Juho Pylvänäinen, Anita Lloyd Spetz. Pulsed Laser Deposition of Metal Oxide Nanoparticles, Agglomerates, and Nanotrees for Chemical Sensors. *Procedia Engineering.* **2015,** 120, 1158–1161.

[30] Roy G. Gordon, Jill Becker, Dennis Hausmann, and Seigi Suh. Vapor Deposition of Metal Oxides and Silicates: Possible Gate Insulators for Future, Microelectronics. *Chem. Mater.* **2001**, 13, 2463–2464.

[31] M. Balog, M. Schieber, S. Patai, M. Michman. Thin films of metal oxides on silicon by chemical vapor deposition with organometallic compounds, *Journal of Crystal Growth*, **1972**, 17, 298-301.

[32] Hongfei Liu, Chandreswar Mahata, Chapter 7 - Metal oxides and metal thin films by atomic layer deposition (ALD), liquid-ALD, and successive ionic layer adsorption and reaction methods for THR applications, Editor(s): Goutam Kumar Dalapati, Mohit Sharma, *Energy Saving Coating Materials, Elsevier,* **2020**, 153-182.

[33] Raija Matero, Antti Rahtu, Mikko Ritala, Markku Leskelä, Timo Sajavaara, Effect of water dose on the atomic layer deposition rate of oxide thin films, *Thin Solid Films*, 2000, 368(1), 1-7.

[34] J. Becker, Atomic layer deposition of metal oxide and nitride thin films, Ph.D. dissertation, Department of Chemistry and Chemical Biology, Harvard University. *ProQuest Dissertations Publishing*, **2003,** 3076871.

[35] Saleem Muhammad Rizwan, Ali Rizwan, Khan Mohammad Bilal, Honkanen Seppo, Turunen Jari. Impact of Atomic Layer Deposition to Nanophotonic Structures and Devices. *Frontiers in Materials*, **2014**, 1, 18.

[36] Peter Ozaveshe Oviroh, Rokhsareh Akbarzadeh, Dongqing Pan, Rigardt Alfred Maarten Coetzee, Tien-Chien Jen. New development of atomic layer deposition: processes, methods and applications, *Science and Technology of Advanced Materials*, **2019**, 20(1), 465-496.

[37] Tuomo Suntola, Atomic layer epitaxy, *Thin Solid Films*, **1992**, 216, 84-89.

[38] Markku Leskela, Mikko Ritala. Atomic layer deposition (ALD): from precursors to thin film structures. *Thin Solid Films.* **2002**, 409(1), 138-46.

[39] Jeong Hwan Han. Growth behavior and characteristics of Ru based electrodes grown by CVD/ALD for next generation DRAM device. *Dissertation thesis*, Department of Materials Science and Engineering, Seoul National University, **2011,** 31-33.

[40] Anjana Devi. 'Old Chemistries' for new applications: Perspectives for development of precursors for MOCVD and ALD applications, *Coordination Chemistry Reviews*, **2013,** 257**,** 3332– 3384.

[41] I. Jõgi. Conduction mechanisms in thin atomic layer deposited films containing TiO_2. *Tartu Univ. Press*, **2007**, 18-39.

[42] Harm C. M. Knoops, Tahsin Faraz, Karsten Arts, and Wilhelmus M. M. (Erwin) Kessels. Status and prospects of plasma-assisted atomic layer deposition. *Journal of Vacuum Science & Technology A*, **2019**, 37, 030902.

[43] Uwai, K. Sequential Self-Limiting Growth of CuO on MgO(100) by Chemical Vapor Deposition. *J. Cryst. Growth,* **1991**, 112 (1), 298–301.

[44] Miikkulainen, V.; Leskelä, M.; Ritala, M.; Puurunen, R. L. Crystallinity of Inorganic Films Grown by Atomic Layer Deposition: Overview and General Trends. *J. Appl. Phys.* **2013**, 113 (2).

[45] George, S. M. Atomic Layer Deposition: An Overview. *Chem. Rev.* **2010**, 110 (1), 111–131.

[46] Guerra-Nuñez, C.; Döbeli, M.; Michler, J.; Utke, I. Reaction and Growth Mechanisms in Al_2O_3 Deposited via Atomic Layer Deposition: Elucidating the Hydrogen Source. *Chem. Mater.* **2017**, 29 (20), 8690–8703.

[47] Knapas, K.; Ritala, M. In Situ Studies on Reaction Mechanisms in Atomic Layer Deposition. *Crit. Rev. Solid State Mater. Sci.* **2013**, 38 (3), 167–202.

[48] Roy Gordon, Precursors with Metal-Nitrogen Bonds for ALD of Metals, Nitrides and Oxides, *Harvard University, Cambridge, MA*. **2005**.

[49] Ellmer, K. Past achievements and future challenges in the development of optically transparent electrodes. *Nature Photon,* **2012**, 6, 809–817.

[50] Panneerdoss IJ, Jeyakumar SJ, Ramalingam S, Jothibas M, Preparation, Characterization, Spectroscopic (FT-IR, FT-Raman, UV and Visible) Investigation, Optical and Physico Chemical Property Analysis on In_2O_3 Thin Films. *J Theor Comput Sci*, **2015**, 2: 120.

[51] Oliver Bierwagen. Indium oxide—a transparent, wide-band gap semiconductor for (opto)electronic applications. *Semicond. Sci. Technol*. **2015**, 30, 024001, 16.

[52] Li S, Xu Q, Zhou Z, Zhao W, Li X, Wen Z, Yao Y, Xu H, Deng H, Dai N, Hao J. Flexible Transparent Heat Mirror for Thermal Applications. *Nanomaterials*. **2020**; 10(12):2479.

[53] Anthony Maho, Sylvain Nicolay, Laura Maria Manceriu, Manceriu Pierre Colson. Comparison of Indium Tin Oxide and Indium Tungsten Oxide as Transparent Conductive Substrates for WO_3-Based Electrochromic Devices, *Journal of The Electrochemical Society*, **2017**, 164(2), H25.

[54] Anil U. Mane, Amy J. Allen, Ravindra K. Kanjolia, and Jeffrey W. Elam. Indium Oxide Thin Films by Atomic Layer Deposition Using Trimethylindium and Ozone. *J. Phys. Chem. C*, **2016**, 120, 9874–9883.

[55] Muhammad Fahad Bhopal, Doo won Lee, Atteq-ur Rehman, Soo Hong Lee, Influence of annealing temperature on structural properties of ITO thin-films on graphite substrate, *Vacuum*, **2016**, 133, 108-113.

[56] N. Balasubmmanian, A. Subrahmanyam. Electrical and Optical properties of relatively evaporated indium tin oxide films *J.Phys. D. Appl. Phys*, **1988**, 22, 279-284.

[57] Ritala, M.; Asikainen, T.; Leskela, H. Enhanced Growth Rate in Atomic Layer Epitaxy of Indium Oxide and Indium-Tin Oxide Thin Films. *Electrochem. Solid-State Lett*. **1998**, 1, 156–157.

[58] Elam, J. W.; Libera, J. A.; Hryn, J. N. Indium Oxide ALD Using Cyclopentadienyl Indium and Mixtures of H_2O and O_2. *ECS Trans.* **2011**, 41, 147–155.

[59] Fumikazu Mizutani, Shintaro Higashi, Mari Inoue, Toshihide Nabatame. Atomic layer deposition of stoichiometric In_2O_3 films using liquid ethylcyclopentadienyl indium and combinations of H_2O and O_2 plasma. *AIP Advances*. **2019**, 9, 045019.

[60] Atomic Limits, "www.atomiclimits.com," Atomic Limits, 8 June 2021. [Online]. Available: https://www.atomiclimits.com/alddatabase/. [Accessed 8 June **2021**].

[61] Sang Bok Kim, Ashwin Jayaraman, Danny Chua, Luke M. Davis, Shao-Liang Zheng, Xizhu Zhao, Sunghwan Lee, Roy G. Gordon. Obtaining a Low and Wide Atomic Layer Deposition Window (150–275^{0}C) for In_2O_3 Films Using an In^{III} Amidinate and H_2O. *Chem. Eur. J*. **2018**, 24, 9525 – 9529.

[62] Polla Rouf, Nathan J. O'Brien, Karl Rönnby, Rouzbeh Samii, Ivan G. Ivanov, Lars Ojamäe, and Henrik Pedersen. The Endocyclic Carbon Substituent of Guanidinate and Amidinate Precursors Controlling Atomic Layer Deposition of InN Films. *J. Phys. Chem. C*. **2019**, 123, 25691–25700.

[63] Nathan J. O'Brien, Polla Rouf, Rouzbeh Samii, Karl Rönnby, Sydney C. Buttera, Chih-Wei Hsu, Ivan G. Ivanov, Vadim Kessler, Lars Ojamäe, Henrik Pedersen. In Situ Activation of an Indium(III) Triazenide Precursor for Epitaxial Growth of Indium Nitride by Atomic Layer Deposition. *Chemistry of Materials,* **2020**, 32 (11), 4481-4489.

[64] NI, "https://www.ni.com," National Instruments, 8 June 2021. [Online]. Available: https://www.ni.com/sv-se/shop/labview.html. [Accessed 8 June **2021**].

[65] Veqter, "www.veqter.co.uk," Veqter Residual Stress Experts, 8 June 2021. [Online]. Available: https://www.veqter.co.uk/residual-stress-measurement/x-ray-diffraction. [Accessed 8 June **2021**].

[66] Malvern Panalytical, "www.malvernpanalytical.com," Malvern Panalytical, 8 June 2021. [Online]. Available: https://www.malvernpanalytical.com/en/products/technology/xray-analysis/xray-scattering/x-ray-reflectometery. [Accessed 8 June **2021**].

[67] Miho Yasaka, X-ray thin-film measurement techniques: V. X-ray reflectivity measurement, *The Rikagu Journal*, 26(2), **2010**.

[68] P. Karthik, V. Vinesh, A.R. Mahammed Shaheer, B. Neppolian, Self-doping of Ti^{3+} in TiO_2 through incomplete hydrolysis of titanium (IV) isopropoxide: An efficient visible light sonophotocatalyst for organic pollutants degradation, *Applied Catalysis A: General,* **2019,** 585(5) 117208.

[69] O. Nilsen, R. Balasundaraprabhu , E.V. Monakhov , N. Muthukumarasamy, H. Fjellvåg, B.G. Svensson. Thin films of In_2O_3 by atomic layer deposition using $In(acac)_3$. *Thin Solid Films*. **2009**, 517, 6320–6322.

[70] M.Thirumoorthi, J. Thomas Joseph Prakash, Structure, optical and electrical properties of indium tin oxide ultra thin films prepared by jet nebulizer spray pyrolysis technique, *Journal of Asian Ceramic Societies.* **2016**, 4(1), 124-132.

[71] Cho S. Structural, optical, and electrical properties of rf-sputtered indium oxide thin films. *Journal of the Korean Physical Society.* **2012**, 60, 2058 - 2062.

[72] Saw KG, Aznan NM, Yam FK, Ng SS, Pung SY, New Insights on the Burstein-Moss Shift and Band Gap Narrowing in Indium-Doped Zinc Oxide Thin Films. *PLoS ONE*, **2015**, 10(10): e0141180.

APPENDIX A

BOM CHECKLIST OF TOOL COMPONENTS: REQUIREMENTS AND CORRESPONDING CODES

Item	Delivered description/ Code	Quantity	Product code/ ID	Supplier
VCR glands (long)	UH-SG-4X6M-191-SLB	X9	6LV-4-VCR-3S-6MTB7	QMT
VCR female nuts	RFN-4-S	X6	SS-4-VCR-1	QMT
Water bubbler:				
i) Single ended cylinder	ZDKCY18-F4N-300-L	X1	304L-05SF4-300	QMT
ii) Valve non-rotating	VS13C-MF4N-RD1-S	X1	SS-16DKM4F4-2	QMT
iii) NPT/6mm connector	DMC-6M-4N-S	X1	SS-6M0-1-4	QMT
iv) Cylinder bottom plug	DP-4-S			QMT
Swagelok T-unions		x2		in stock
Swagelok unions 6mm	DU-6M-S	X13	SS-6M0-6	QMT
Swagelok 4-way fitting/ Union cross	DX-6M-S	X1	SS-6M0-4	QMT
Swagelok Back Ferrules	DFB-6M-S	X10	SS-6M3-1	QMT
Swagelok Front Ferrules	DFF-6M-S	X10	SS-6M4-1	QMT
Swagelok Union Tee Gas tube	UH-WT-6M-191-SLB	X2	316L-6MTB7-3	QMT
CA to flowlink valve connector	compressed air to 'ALD' valves	X4		in stock
Flowlink valves with VCR connection	Flowlink	X4		in stock
HAM-LET needle valves	H-300U-SS-L-V-6MM-RS	X1	H-300U-SS-L-V-6MM-RS	in stock
HAM-LET needle valves (red aluminum handle)	VMH-D-4T-RD-S	X4	H-300U-SS-L-V-6MM-RAR	QMT
KF25 centering rings	KF25/R	x5		Rowaco
KF25 clamping rings	KF25/C	x5		Rowaco
KF25 to 40 reducer	KFA25/40	X1		Rowaco
Flexi stainless steel hose	KX25/500	X1		Rowaco
KF40 manual valve - VIV40KF	to control pump flow	X1		Rowaco
Plastic pipe	4mm	10m		in stock
Gas pipe (metal)	6mm	X1		in stock
Heating tapes	enough to be wound from bubbler to oven inlet	1x1.5m 2X3m	S015 S030	Hemi Heating
Compact DAQ Chassis	CDAQ-9171	X1	(781425-01) with 1 USB slot	NI
Module 8 channel, screw terminal	NI 9472	X1	(779004-02) conformal coated sourcing DO module	NI
Power Supply to DAQ unit 24V, 0.6A	Siemens LOGO! 6EP3330-6SB00-0AY0	X1		Automation 24
Festo EPC (Manifold rail for in-line valves)	VTUG-10-SK8-S1H-Q6L-UR-Q4S-KKLL+H	X1	VTUG-10-SK8-S1H-Q6L-UR-Q4S-KKLL+H	Festo
Deposition chamber	Heating oven with a temperature read out	X1		In stock

Vacuum pump	Connected to the stainless-steel tube of the deposition chamber	X1	VARIAN DS 302 (model 949-9325)	In stock
Stainless steel tube	With inlet for reaction gases and outlets for substrate loading and unloading, pressure gauge and pump exhaust	X1		In stock
Digital thermometers	For temperature measurement on the metal precursor bubbler and the delivery lines	X5	Model 14-649-79,11799725. Kangaroo thermometer Only 2 or 3 in use at a time	Fisher Scientific
Pressure gauge	With KF16 coupplings connected to the stainless-steel tube outlet	X1	EPIGRESS 0-1000mbar	In stock
Feedthrough thermocouple	With air and vacuum side connectors and 1m bare thermocouple wire (to measure actual substrate temperature)	X1	DN25KF, TYPE K.	Rowaco
Manual Y-Inline valve	For manual pressure control to the pump	X1	NW40KF OD=38.1	Rowaco
Plug-in dimmer	For heating tape temperature control	X1	LED 0-200W	Ljustema
Flexible plastic	Connection between pump and deposition chamber. Made of plastic to prevent pump vibrations from reaching deposition chamber	X1		In stock

APPENDIX B
ALD TOOL LAYOUT

Set up idea is a hot wall crossflow reactor system design with ALD valves controlled by LabVIEW

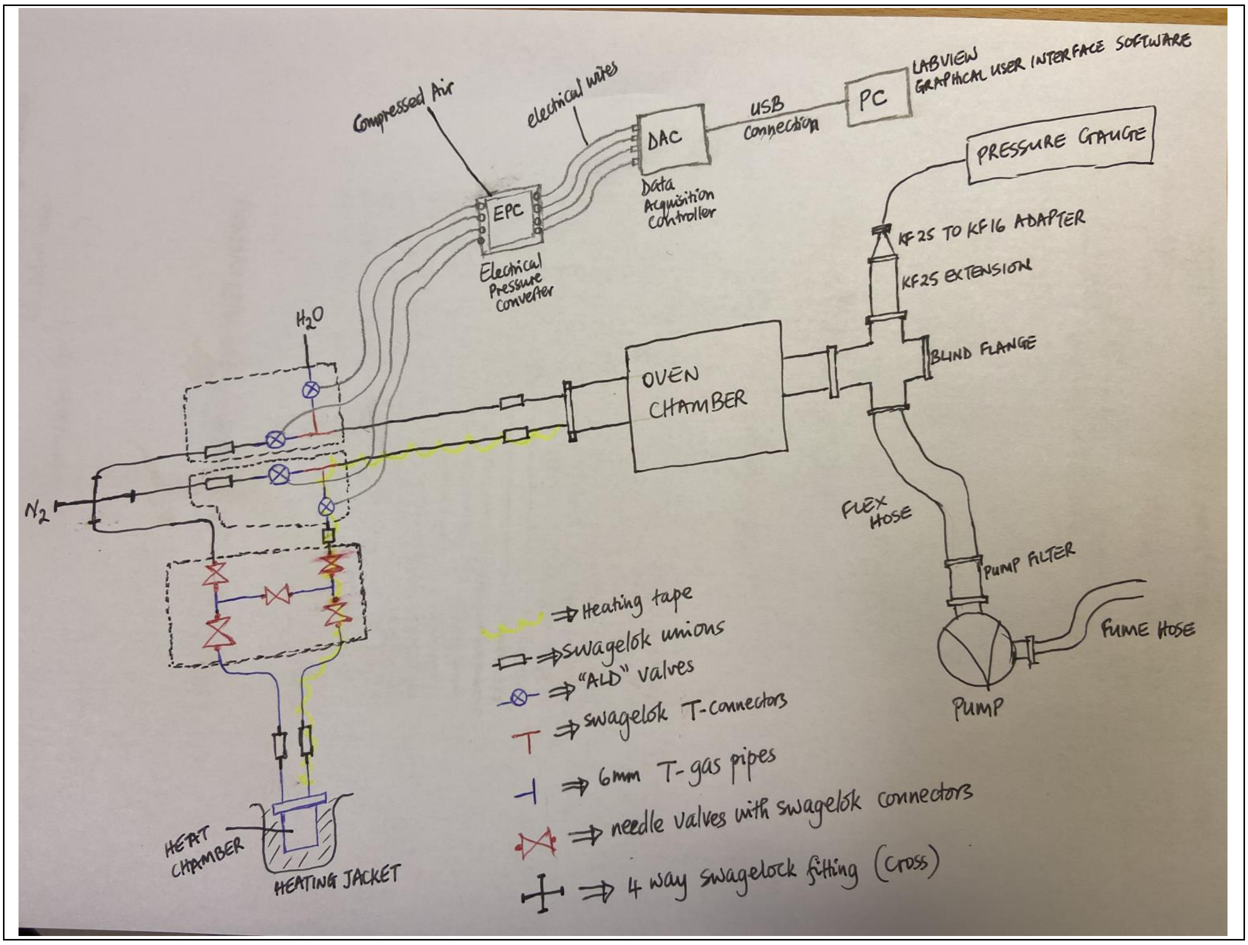

APPENDIX C
ASSEMBLING THE TOOL

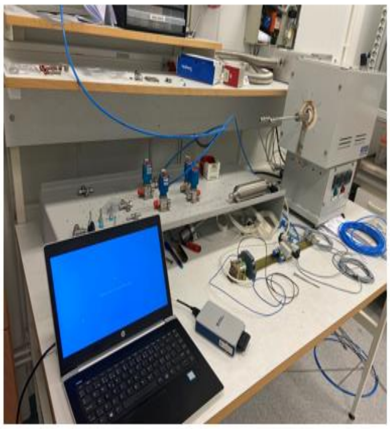

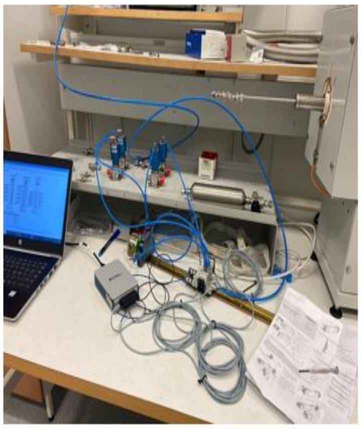
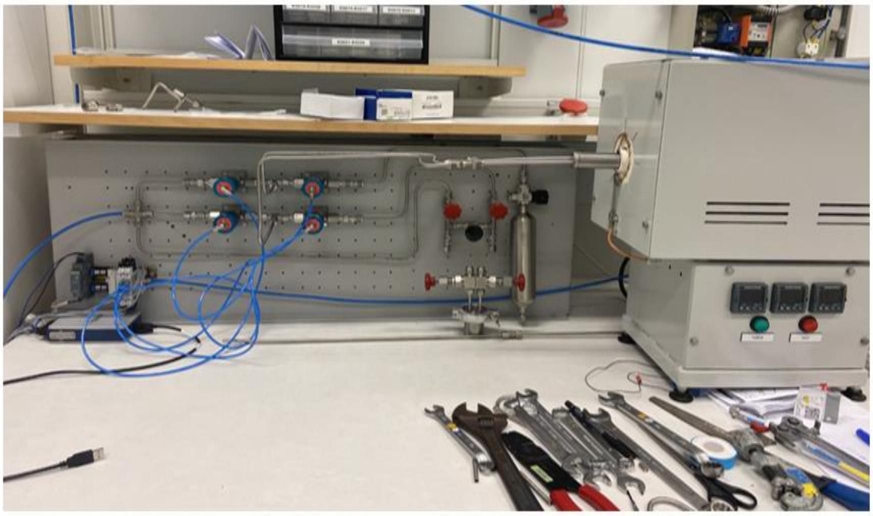

APPENDIX D

LABVIEW CODE MANUAL

1. Launch **LabVIEW** by double clicking the above logo: on the desktop, taskbar or by searching 'LabVIEW' in the windows search bar.

2. Launch **'ALD_control_system 2**' by selecting and doubling click it or selecting 'open'.

3. Press 'Run' (➡) to start the graphical user interface (GUI)

4. Input your '**Program Settings'** by typing in your required process specifications:
   i) Number of cycles that you want the program to run.
   ii) Time you want each valve to be open/ closed, depending on your dose time and pipe cleaning time for whichever precursor/reactant and pipe you want, respectively. Please note that ONLY ONE of the 4 valves is open at any given time!
   iii) Indicators on both the front panel of the GUI and the hardware (FESTO manifold) will show which valve is open in real time.

5. Use the '**Manual Valve Control'** buttons to get manual control of each valve. For example, pressing '*clean both pipes'* gives manual cleaning by opening both pipes for nitrogen gas to flow through them.

6. Once the program is running and all parameters set, you can click **'Start'** and the indicators on the panel will show you if the program is running or has finished by turning between lime and dark green colors. In this section you can also see time left to finish the run as well as the cycle number that is currently running.

7. It is not recommended, but possible, to **'Pause'** or **'Abort'** the program using the respective buttons.